Girão Coelho AM, Mottram JT, Harries KA (2015). *Finite element guidelines for simulation of fibre-tension dominated failures in composite materials validated by case studies*. Composite Structures 126, 299-313

Finite element guidelines for simulation of fibre-tension dominated failures in composite materials validated by case studies

Ana M. Girão Coelho

Marie-Curie IEF Research Fellow
(corresponding author, a.m.girao-coelho@warwick.ac.uk)
Civil Research Group, School of Engineering, University of Warwick
Coventry CV4 7AL, UK

J. Toby Mottram

Professor
(j.t.mottram@warwick.ac.uk)
Civil Research Group, School of Engineering, University of Warwick
Coventry CV4 7AL, UK

Kent A. Harries

Associate Professor
(kharries@pitt.edu)
Department of Civil and Environmental Engineering, Swanson School of Engineering,
University of Pittsburgh, Pittsburgh PA 15261, USA

Abstract

This paper presents a finite element modelling methodology to predict the initiation and damage progression in notched composite laminated plates subjected to increasing in-plane tension load. An important feature of the methodology is it does not rely on customized user-subroutines but solely on the analysis capabilities of the general purpose software Abaqus; thus ensuring that the numerical results can be universally reproduced. The methodology presented copes with intralaminar failure modes and uses the Hashin failure criterion to predict the onset of failure (cracking). To account for damage progression after crack initiation there is a fracture energy calculated for each of four failure modes. Four open-hole laminated plates taken from the literature are used for benchmark examples. The predicted ultimate strength based on the analytically-obtained stress-displacement curve was found to be within 10% of the experimental observations. To study the influence of the interaction of having two or three holes across the mid-plane of a pultruded open-hole tension specimen, a parametric study was carried out. The paper ends giving guidelines for the generalized modelling methodology using Abaqus without user-subroutines.

Keywords: Damage mechanics; Fibre-tension failure; Finite element modelling; Open-hole tension; Pultruded material.

1. Introduction

Composite structures of fibre reinforced laminae that are commonly found in aerospace, automotive and civil engineering applications exhibit a distinctively nonlinear behaviour when deformed to ultimate failure. This nonlinearity arises in various ways. The heterogeneous nature of the laminae, which consists of fibres of one material (usually carbon or glass) in a matrix of another (typically a polymer resin), makes the mechanical behaviour complex. The constitutive stress-strain response has directionally dependent properties and the failure behaviour is typically brittle in nature. In addition, since many composite structures consist of flat or curved thin plate elements, they are likely to undergo large deflections.

The description of real composite behaviour is a challenge, either using experimental procedures, or numerical methods. In this respect, virtual tests of composite materials carried out by means of numerical modelling are increasingly replacing some mechanical and physical tests to predict and substantiate structural performance and integrity. Computational advances in fracture modelling, especially the improvement of cohesive models of fracture and the formulation of hybrid stress-strain and traction-displacement models that combine continuum and discrete material damage representations in a single calculation, for example, make such a virtual approach realistic.

Finite element simulations can be performed at any scale level of the structural composite. Fig. 1 illustrates the cross-section of a laminate having unidirectional laminae (or plies, or layers) modelled at three different scales: (i) microscale (constitutive modelling of fibre and matrix), (ii) mesoscale (lamina level as a multiphase homogenized material), (iii) macroscale (laminate modelled as a series of stacked unidirectional laminae). In this paper, modelling is performed at the mesoscale at which the lamina is considered to be a homogeneous continuum. In other words, the material is homogenized by smearing the behaviour of the fibres and the matrix over a single lamina.

In order to obtain meaningful and reliable finite element simulations, analyses must account for different failure (or damage) processes and their progression and interaction. Cracking of the matrix parallel to the fibres may occur, as well as fracture of the fibres in tension and kinking or buckling of the fibres in compression, possibly accompanied by debonding at the fibre-matrix interface. Matrix failure can be classified as delamination failure when it occurs between adjacent laminae. Early matrix cracks and delamination at free edges are mainly caused by the low transverse

stiffness, and the mismatch of the Poisson's ratios between layers with different fibre orientations. Matrix-dominated processes correspond to the onset of damage in most composite designs, but do necessarily lead to loss of structural integrity. Further load can be accommodated due to stress redistribution in the laminate. This introduces the concept of progressive failure (or damage) of the composite material. In this framework, the numerical models presented here are based on critical stress and/or strain combinations that trigger damage initiation, and critical energy release rates or damage mechanics considerations that describe damage propagation. As this process progresses from meso- and macroscale to a large composite structure, the result is a continued weakening of the entire structure, up to the point where the structure can no longer carry additional load. This process is highly nonlinear as it degrades the ply and the laminate stiffness and extends beyond failure initiation.

Current state-of-the-art for computational modelling of progressive failure of composites is based almost exclusively on composite architectures found in aerospace and automotive applications (so-called *advanced composites*). This research work quantifies the state-of-the-art for materials produced by the pultrusion method, which are generally used in civil and infrastructural applications. The intent is therefore to enable and support the development of structural design guidelines. Pultruded shapes are different to thin-walled advanced composite structures in so far as they are typically prismatic, have relatively thicker component plates, and typically have lengths in the direction of pultrusion at least an order of magnitude greater than the section dimension. Indeed, Turvey and Wang [1] reported that methods of analysis appropriate for aerospace composites are "not suitable" for pultruded plates typical of infrastructure applications. They appear to attribute the inappropriateness of the methods to the more variable nature of infrastructure materials.

In civil applications, the matrix typically consists of a thermoset resin (e.g. polyester or vinylester) and additives (e.g., for colour, fire resistance, etc.). E-glass unidirectional rovings and continuous filament mats are used for the reinforcement, with an overall volume fraction typically between 30 and 50%. The fibres in the continuous filament mats are long, swirl and are randomly oriented in the plane. It is assumed the mats represent a layer with isotropic in-plane mechanical properties.

As the motivation increases to use pultruded shapes in construction, researchers are urged to investigate the sensitivity of these materials to damage, and to characterize the various mechanisms that govern the onset and progression of damage, leading to ultimate failure. There are a number of sources of initial damage, the most relevant being delamination and notches. Through-thickness holes – effectively notches – are drilled to mechanically fasten parts in the structure. The introduction of notches leads to stress concentrations in the composite material that cannot be redistributed by plastic flow, as would be the case if the material possessed inherent ductility.

Designers need to know whether damage will develop and propagate under loading in the presence of the stress-raiser in order to assess structural integrity. There are a variety of theories and numerical implementations with respect to the modelling of progressive damage and failure in advanced composites. In the present research, the smeared crack approach will be adopted which, when properly implemented, ensures a large degree of objectivity with respect to finite element discretization and requires little or no modification to standard commercial finite element codes, such as Abaqus [2]. This latter aspect is particularly relevant to practising engineers concerned with virtual testing related to structural integrity and damage tolerance of fibre reinforced polymers for safety-critical structures.

2. Failure analysis in the context of the finite element method

The numerical modelling of composite structures in the elastic range is quite straightforward. However, the nature of failure initiation and progression to rupture, involving matrix, fibre and/or interface damage and fracture, makes full behaviour analysis rather complex. External loads are predominantly carried by axial forces in the fibres, and the failure process is driven by the energy released as these are unloaded after fracture. Matrix-dominated failure mechanisms, in the form of cracks and delaminations joining-up to produce a fracture surface, occur without necessarily having to break fibres.

Typical constitutive behaviour is characterized by an initial linear response followed by a second nonlinear response having reduced stiffness that results from the formation of micro-cracks in the vicinity of the crack tip. The strain energy accumulated in the material is released at the peak-load and a stable crack propagates progressively with a reduction in strength and stiffness until eventual failure. This is a typical quasi-brittle behaviour, although most polymer-based matrices can deform plastically before damage when subjected to shear loading. This progressive damage modelling is carried out in three steps [3]:

1. Stress analysis by finite element modelling and simulations: the geometry of the structure, load history and initial boundary conditions being known, the fields of stress and strain are calculated by means of strain constitutive equations and a numerical procedure.
2. Failure criterion or criteria: the most critical location(s) with regard to fracture is (are) determined and, the load corresponding to this macro-crack initiation is calculated by integration of damage constitutive equations for the history of local stress or strain.

3. Degradation of material/laminate properties based on damage progression models to calculate the evolution of the critical macro-crack(s) up to final rupture of the whole structure.

This section reviews the main features for the finite element modelling of intralaminar failure in a laminated plate. Some of the key concepts are considered first, including the element types and the material parameters. The mechanisms by which laminates may fail are then discussed. The different approaches for the modelling of such mechanisms are considered. Numerical aspects to the effective application of the progressive damage modelling are finally discussed.

2.1. Key concepts

2.1.1. Element types

An efficient geometric modelling must account for the non-homogeneous and layered nature of the laminate. The finite element model must firstly represent the lamina orientation, stacking sequence and thickness variation, and secondly provide an adequate representation of the global stress field, the through-thickness stress variations, local stress concentrations and failure modes. The analysis must therefore be treated as being three-dimensional. Solid (brick) elements with one layer of bricks representing each lamina can be used although this approach is not practical because the analysis is computationally expensive if the layup has more than just a few laminae. Additionally, conventional solid elements show an overly stiff behaviour and effects of locking, especially the Poisson thickness locking effect, when used in very thin applications [4]. In practice, it is usual to employ shell elements, particularly in the form of *continuum shells*, which are elements that have the geometry of bricks but their kinematic and constitutive behaviour are similar to those of conventional shell elements. Continuum shell elements are able to reliably reproduce results in simulations of thin-walled structures by means of only one element over the thickness when higher-order displacement fields are used. First approaches of this kind assumed a constant strain field through the thickness [5,6,7] and were later extended by considering an additional set of internal degrees of freedom to add a quadratic term to the displacement field that allowed for a linear variation of the strain field through the thickness [8].

2.1.2. Material parameters

A unidirectional lamina is an orthotropic material whose planes of symmetry are parallel and transverse to the fibre direction. The material coordinate axes are conventionally designated by the

principal axes 1, 2 and 3, representing parallel- and transverse-to-fibre directions and the through-thickness direction, respectively.

The mechanical behaviour of a lamina in a continuum modelling approach is characterized by means of a constitutive law that includes, for damage-based material models, the following three sets of material properties:

1. A law for the elastic behaviour of the lamina, which is idealized as a homogeneous material by smearing the discrete properties of the fibre and matrix, based on the transversely isotropic version of Hooke's law [9]. The relevant engineering constants for the unidirectional reinforcement are the moduli of elasticity in the fibre and transverse directions, E_1 and E_2, the longitudinal (major) and transverse (minor) Poisson's ratios, ν_{21} and ν_{23}, and the longitudinal (in-plane) and transverse shear moduli, G_{12} and G_{23}.
2. Lamina longitudinal, transverse and shear strengths comprise [10]:
   $f_{1,T}$: axial strength in tension; $f_{2,C}$: transverse strength in compression;
   $f_{1,C}$: axial strength in compression; $f_{1,S}$: shear strength in the axial direction;
   $f_{2,T}$: transverse strength in tension; $f_{2,S}$: shear strength in the transverse direction.
3. Fracture energy (or fracture toughness), G_c in the above directions [11,12]. G_c governs crack growth and is defined as the work needed to create a unit area of a fully developed crack.

2.2. Intralaminar failure modelling

The intralaminar failure mechanism is characterized by matrix cracks that run parallel to the fibres and propagate through the thickness of the laminate (rather than the laminae), shear in the transverse or longitudinal directions, and fibre breaking cracks, as can be seen in Figs. 2a-c [13]. In these figures, mode 1 represents a failure mechanism in the longitudinal direction and mode 2 in the transverse direction. T, C and S stand for tension, compression and shear, respectively. Matrix failure mechanisms are usually the first form of damage observed with fibre fracture marking the ultimate failure in a well-designed laminate. In fact, fibre fracture can be seen as the *only desirable* fracture mechanism, since the reinforcement is the principal load carrying constituent. In Figs. 2a and 2b the fracture surfaces caused by transverse compression and transverse shear are illustrated too. The fracture angle of ±35° to ±40° in a unidirectional lamina is typical for pure transverse compression [14]. The fracture angle for pure transverse shear is approximately 45°. This fracture behaviour is well-known for brittle materials.

Continuum damage mechanics models for the prediction of intralaminar failure are used in this work with a range of examples on different applications. The damage mechanics of composites is the modelling of the initiation and degradation phenomena at a mesoscale. At this scale, the laminate is modelled as a stacking of homogeneous layers that may be connected by interfaces that model delamination. Relative variations of stiffness are the damage indicators. The progressive transverse matrix cracking and the brittle fracture of fibres are included at the single lamina level. The damage state at every (1,2) point in the plane of the plate is assumed to be uniform within the layer thickness.

2.2.1. Damage initiation theories for plies

Literature presents phenomenological and physically-based failure initiation criteria for a lamina. Phenomenological criteria have been proposed by extending and adapting failure theories to account for the anisotropy in stiffness and strength, but they do not reflect the level of complexity that is inherent to this type of structural material. Underlying such complexity is the fact a lamina consists of mechanically dissimilar constituent phases: stiff elastic brittle fibres and a compliant yielding matrix. Physically-based criteria distinguish between states of stress not leading to fracture and those implying fracture.

The Tsai-Wu interactive (phenomenological) criterion [15] is the most commonly adopted in research methodologies, and essentially consists of a single relation for the interaction of the different internal stress components, σ_i, in the three-dimensional material frame. For a general anisotropic material the failure surface in the stress-space has the following scalar form:

$$F_i\sigma_i + F_{ij}\sigma_i\sigma_j = 1 \quad \text{and} \quad F_{ii}F_{jj} - F_{ij}^2 \geq 0 \tag{1}$$

in which F_i, F_{ij} are strength tensors of the second and fourth rank, respectively. The following contracted notation is used in the above equation: $i, j = 1, 2, \ldots 6$.

The first failure theory that makes a clear distinction between the different lamina failure modes was developed by Hashin and Rottem [16], and later modified by Hashin [17] to predict the onset of damage. This theory consists of the following expressions:

Fibre in tension $$\frac{\sigma_1}{f_{1,\mathrm{T}}}=1$$

Fibre in compression $$\frac{\sigma_1}{f_{1,\mathrm{C}}}=1$$

Matrix in tension $$\left[\frac{\left(\sigma_2+\sigma_3\right)^2}{f_{2,\mathrm{T}}^2}+\frac{\tau_{23}^2-\sigma_2\sigma_3}{f_{2,\mathrm{S}}^2}+\frac{\tau_{31}^2+\tau_{12}^2}{f_{1,\mathrm{S}}^2}\right]^{\frac{1}{2}}=1 \qquad (2)$$

Matrix in compression $$\left[\left[\left(\frac{f_{2,\mathrm{C}}}{2f_{2,\mathrm{S}}}\right)^2-1\right]\frac{\sigma_2+\sigma_3}{f_{2,\mathrm{C}}}+\frac{\left(\sigma_2+\sigma_3\right)^2}{4f_{2,\mathrm{S}}^2}+\frac{\tau_{23}^2-\sigma_2\sigma_3}{f_{2,\mathrm{S}}^2}+\frac{\tau_{31}^2+\tau_{12}^2}{f_{1,\mathrm{S}}^2}\right]^{\frac{1}{2}}=1$$

whereby σ_i and τ_{ij} (i, j = 1,2,3) are the principal stresses for the lamina. The failure criterion used to predict matrix tensile and compressive cracking includes the shear stresses that may lead to matrix shear failure, as can be seen in Eqs. (2c-d). The Hashin criterion is employed herein to predict damage onset and the governing failure mode within a lamina. This criterion has been shown by many researchers to be easily implemented in finite element analyses and requires lamina properties that can be fairly easily determined on an experimental basis. Furthermore, it has provided numerically reliable results when applied to predict the *first ply failure load* in both carbon fibre and glass composites. In most cases, the laminate can carry a greater load because it possesses damage tolerance prior to complete rupture. It is often the case that a sequence of lamina failures occurs under increasing stress before rupture of the entire laminate at the *last ply failure load*.

2.2.2. Damage progression models

For composite structures that can accumulate damage, the use of failure initiation criteria is not sufficient. The rate and direction of damage propagation defines the damage tolerance of the structure and its final damage state. Consequently, once a failure initiation criterion is satisfied, the associated damage variable is different from zero and further loading will cause degradation of the material stiffness coefficients. The challenge is to choose appropriate combinations of failure criteria and degradation models. These models can be divided into two main groups:

1. Heuristic models based on a ply-discounting material degradation approach [18,19].
2. Progressive failure models based on continuum damage mechanics [12,20-25].

The classical *ply discount method* assumes that a failed ply cannot take any further load. In reality, a fractured ply can exhibit significant residual load-carrying capacity. The approach of *progressive failure analysis* is to assume that all material nonlinearity is due to damage in the form

of reduced stiffness. Accordingly, the majority of existing models for progressive intralaminar failure analyses are based on softening constitutive models that use scalar damage variables or mode-specific strain energy release rates (fracture toughness) and total dissipated strain energy [22,26-28]. Displacements due to crack opening are smeared over a characteristic element, as described in Section 2.3. The shape of the softening law is often assumed to be inconsequential for the prediction of fracture, provided that it is defined as a function of the fracture toughness [29].

The approach used in this research work is based on the energy requirement for the deterioration of stiffness within a characteristic or unit volume per unit time. It also assumes that the strain energy dissipates gradually as damage develops. Damage evolution laws are defined for the various possible failure modes (Fig. 2). Each damage evolution law includes the corresponding fracture toughness, representing the energy dissipated by inelastic processes in the fracture process zone. Guidelines for the evaluation of these properties are summarized in [12] and [24].

2.2.3. Simulation of progressive damage in Abaqus

The continuum damage model implemented in Abaqus [2] predicts the onset and accumulation of intralaminar damage mechanisms, as well as final structural collapse by the propagation of a macro-crack. For this modelling, the Hashin criterion, given in Eq. (2) and defined in Abaqus as parameters HSNFTCRT, HSNFCCRT, HSNMTCRT and HSNMTCRT, respectively, is used for damage initiation. A specific mode of failure is predicted when the corresponding parameter reaches a unit value. The damage progression is tracked, from 0 to 1, using the Abaqus options DAMAGEFT, DAMAGEFC, DAMAGEMT, and DAMAGEMC, respectively.

The influence of damage on the constitutive model is based on the work of Matzenmiller *et al*. [21]. A drawback of this damage progression model is that it does not reproduce localization of the tensile fracture properly. This aspect is resolved by means of the crack band approach [30]. The *crack band model* uses a modification of the post-peak part of the constitutive law (damage progression) to enforce the energy dissipation as determined by experiments by a localized crack band.

2.3. Regularization in quasi-static regime

The underlying mathematical problem of damage-induced deformation localization is that of an ill-posed boundary-value problem; that is, a system of ordinary differential equations with solution and derivative values specified at different points. In general, numerical methods for analysing and solving ill-posed problems include a so-called *regularization parameter*, which controls the degree

of smoothing (or regularization) applied to the problem. The technique involves a mathematical scheme called *localization limiter*, in order to avoid *size effects* and *numerical instability*.

Failure occurs by progressive damage that involves strain localization processes that result in a sharp decrease of the load-carrying capacity. Strain localization is a concept that describes a deformation mode, in which the deformation of a structure occurs in one or more narrow bands, referred to as the fracture process zones. The formation of these bands is accompanied by a softening response, usually leading to complete collapse. The width and direction of localization bands depend on the material parameters, geometry, boundary conditions, internal stresses/strains, loading distributions and loading rate. As a consequence, numerical predictions using continuum damage mechanics are found to be strongly dependent on the size of the finite element mesh used. This problem is known as *spurious mesh sensitivity*: the energy that is released by cracking damage depends on the mesh size and tends to zero in the limit of an infinitesimally refined mesh. To overcome this difficulty, the material constitutive model must be supplemented with some mathematical condition that prevents localization of smeared cracking into arbitrarily small regions [31]. *Nonlocal* damage theories have emerged as an effective means for capturing size effects. These theories relate the stress at any point to the state of deformation within a finite volume about that point [32-34]. The simplest, and computationally most effective nonlocal approach is the *crack band model* [30]. The model ensures the correct energy dissipation in a localized damage band by rescaling the energy of the post-localization part of the stress-strain relationship by taking the size of the finite elements into account [32]. The crack band model provides only a *partial regularization* of the problem; it is not a true localization limiter, as it allows the global response characteristics to be truly captured, but the width of the numerically resolved fracture process zone is still dependent on the mesh density [35]. In this context, Bažant and Oh [30] derived the critical size l^* (element characteristic length or length of the fracture process zone) by adjusting the energy dissipated by each failure mechanism M:

$$l^* \leq \frac{2E_{\mathrm{M}}G_{\mathrm{M,c}}}{f_{\mathrm{M}}^2} \tag{3}$$

where E_{M}, $G_{\mathrm{M,c}}$ and f_{M} are the relevant modulus of elasticity, fracture energy and strength, respectively. Bažant and Oh [30] suggest a practical critical size of about half of that determined from Eq. (3).

The crack band model performs best if the path of the fracture process zone is known in advance (e.g., tension failure of notched laminates), and if the mesh is designed to coincide with this zone.

Strain-softening constitutive models cause additional convergence problems when using global solution methods because the tangential matrix of the softening material ceases to be positive definite. This leads to lack of robustness in the equilibrium iterations. Such *numerical instabilities* can be prevented by adding *viscosity* to the constitutive model (i.e., rate-dependent behaviour). The *artificial viscosity regularization* leads to corresponding stiffness matrices that have stable equilibrium iterations. This approach was first proposed to overcome this type of problem when analysing fracture processes in metals [36] demonstrating how introducing viscous terms in damage laws could be a convenient way to regularize the ill-posed problems of rate-independent laws.

In this contribution, the general framework of viscous regularization is adopted, as recommended by Abaqus with its composite damage model. Because this involves a nonphysical rate dependence, additional effort in model calibration and validation is necessary. Values for this parameter are generally determined by using inverse modelling techniques since it cannot be explicitly related to any physical quantity. Successful implementation of artificial viscosity in continuum material models to improve the convergence of the numerical algorithm has been demonstrated [23,37].

2.4. Nonlinear solution process

The nature of a progressive failure methodology requires a nonlinear implicit or explicit solver to establish equilibrium. In implicit formulations, the current stress state and a consistent local tangent material stiffness matrix are needed to form the internal force vector for the residual force vector computation, to generate the Jacobian matrix, and to solve the set of algebraic equations at every time step using a Newton-Raphson-like method. In explicit formulations, only the current stress state is needed to evaluate the current internal force vector in order to advance the transient solution forward in time. Explicit solvers do not need to form a global stiffness matrix because the linear equations are not solved simultaneously for the entire system (like in implicit methods), but the stress wave propagates from element-to-element.

Abaqus implements both implicit (Abaqus/Standard) and explicit (Abaqus/Explicit) solvers. The implicit solution strategy is suitable for problems involving smooth geometric and material nonlinear analyses. The geometric nonlinearity is due to large strain and large rotation kinematics. The nonlinear material behaviour is due to the degradation of the mechanical properties of the laminae and the matrix-rich layer between laminae to simulate intralaminar and interlaminar damage mechanisms. A load stepping routine is used in Abaqus/Standard. There is no restriction on the magnitude of the load step as the procedure is unconditionally stable. The increment size

follows from numerical accuracy and convergence criteria. Within each increment, the equilibrium equations are solved by means of the Newton-Raphson method, which is stable and converges quadratically. In this method, for each load step, the residuals are eliminated by an iterative scheme in which the load level remains constant and the structure is analysed with a redefined tangent stiffness matrix. The accuracy of the numerical solution is measured by means of appropriate convergence criteria. Their selection is of the utmost importance. Too tight convergence criteria may lead to an unnecessary number of iterations and consequent higher computational cost, while too loose a tolerance may result in incorrect or inaccurate solutions. Generally speaking, in nonlinear geometric analyses, relatively tight tolerances specific to the problem are required, while in nonlinear material problems looser tolerances are admitted, since high local residuals are not easy to eliminate. Abaqus/Standard additionally provides the option of including a *line search algorithm* [38] to improve the robustness of the Newton-Raphson method.

With respect to the incremental method, a load curve is defined. Loads should be applied to the specimen in a displacement-control fashion thus enforcing a better conditioning of the tangent stiffness matrix when compared to the classical load-control procedure.

Explicit schemes offer a more robust alternative for convergence of quasi-static load cases but may come at an even higher computational cost as smaller solution time steps are required. Additionally, to mitigate unwanted inertial effects, the time step must be less than a critical value based on the highest eigenvalue in the model. The stable time increment Δt_{stable} is the minimum time that a dilatational wave takes to move across any element in the model, and is given by:

$$\Delta t_{\text{stable}} = l^{*}\sqrt{\rho / E_1} \tag{4}$$

where ρ is the material density. The stable time steps for quasi-static explicit analyses are very small, on the order of 10^{-8} seconds or less, and the entire calculation process requires hundreds of thousands of increments. Mass scaling and damping are common approaches to assist in artificially reducing the computational cost. Quality checks, such as the ratio of kinetic energy to internal energy must be carried out to ensure that the problem remains essentially quasi-static. An acceptable rule of thumb is to set acceptance of this ratio to 0.01~0.05.

3. Benchmark applications

The numerical studies presented in this section include a continuum damage approach to modelling advanced composites. Continuum damage models address the failure mechanisms from a global view, where individual damage mechanisms are homogenized and constructed around a failure criterion. This approach is the least complex and uses the composite layup modeller tool within the Abaqus pre-processor to define the individual plies through the laminate thickness. However, this method does not allow delamination between plies to be modelled; only intralaminar damage modes for calculating the progression of the damage path are considered. Experimental and numerical results available from literature on carbon/epoxy composites are used for calibration and validation of the proposed models.

Open-hole tension (OHT) laminates under in-plane tensile loading are considered. The OHT for composite materials is a challenging problem because failure involves complex mechanisms such as fibre breakage, matrix cracking and delamination (the latter is not modelled in the current work as it has not been experimentally observed in these benchmark cases). In addition, the OHT strength and dominant failure modes can depend on geometric parameters, such as hole diameter, stacking sequence and ply thickness, and material properties

3.1. Examples

Rectangular plates with a centrally placed, circular hole subjected to in-plane tensile loading, known as OHT specimens, are considered as examples of intralaminar failure. Only one half the specimen is modelled due to symmetry about the longitudinal axis. The geometric data for the OHT test specimens is taken from Chang and Chang [39], and is shown in Fig. 3. Four different stacking sequences are considered, corresponding to layups of $[0/\pm45/90_7]_s$, $[0/(\pm45)_2/90_5]_s$, $[0/(\pm45)_3/90_3]_s$, and $[(\pm45)_6]_s$. Reported material properties are given in Table 1 [37,39]. Viscous regularization was added to the constitutive model with a viscosity coefficient of 1×10^{-5}, which was found to be sufficiently small for accurate modelling.

The laminates were modelled with reduced integration continuum shell elements (SC8R in Abaqus) that offer a computationally efficient method to simulate systems that are globally three-dimensional, yet locally planar, as is the case with multi-layered composite structures. One integration point per ply was used in the laminate mesh specification, which was divided into a coarse mesh area away from the hole and a refined mesh around the hole and in the direction of loading. A mesh refinement study was carried out to confirm that the model results converge to the

experimental [39] and to previously reported numerical predictions [37] at the selected mesh density. The study was conducted for the four different layups with respect to two parameters: the degree of mesh discretization, in order to represent the tensile-dominated problem, and the number of elements through-the-thickness. It was found that a single element through the thickness *t* was sufficient to capture the through-the-thickness deformation. This strategy is appropriate for continuum modelling of the OHT specimen that is assumed to behave in a plane stress condition, because the formation and propagation of delamination zones between the laminae, which include out-of-plane stress states, are not permitted. In this case, continuum shell elements can have large aspect ratios (on the order of hundreds-to-one).

Boundary conditions consistent with the actual plate restraints are applied (Fig. 3). Displacement boundary conditions restraining movement in the thickness direction at the edges of both ends were also added. Displacements in the transverse direction were restrained along all surfaces on the centre line of the model to comply with geometric symmetry. The load was applied monotonically by imposing incremental axial displacements at the unrestrained end during the analysis to achieve the required range of laminate stresses. The analysis was performed using a global stabilization factor of 2×10^{-4}, which corresponds to the code default.

3.2. 0°/90°/±45° based layups

The first validation example is the $[0/(\pm45)_2/90_5]_s$ laminate for which collapse is governed by a tension-failure mode. A first analysis is run using the default implicit Abaqus solver. The obtained tensile stress (i.e. the applied load averaged over the nominal gross cross-section) versus end displacement curve is plotted in Fig. 4 as a solid line and compared with the maximum experimental stress (horizontal dashed line) obtained by Chang and Chang [39] and the finite element results (light solid line) of Maimí *et al*. [37], who implemented a specific damage model in Abaqus/Standard using a user-subroutine UMAT [2,37]. In this work, we choose not to develop our own subroutines and rely solely on the analysis capabilities of Abaqus so that the results reported can be reproduced by any analyst. Stresses are computed based on the nominal width and thickness. For the model developed in this work, the corresponding fibre-tension damage plots, measured by the parameter DAMAGEFT [1] at specific stress levels on the loading history, indicated by A and B on the curve in ~Fig. 4, are illustrated in Fig. 5. Complete fibre-tension damage is predicted when DAMAGEFT = 1. Several remarks can be made. Firstly, the predicted tensile strength does not correlate well with the experimentally determined strength [39] by 76%. Secondly, the nonlinear numerical response is characterized by an initial elastic phase, followed by a loss of stiffness

(segment AB) until rupture allows rapid stress relief. This curve is not characteristic of the brittle failure anticipated for this particular OHT specimen. Thirdly, Fig. 6 highlights a mesh instability phenomenon, known as hourglassing, which is a spurious (singular) deformation mode characteristic of reduced integration elements, and is a mathematical artefact since it is for zero energy deformation. Finally, it can be concluded from the simulation results that the Abaqus model is not simulating the damage initiation and propagation reliably. Owing to the stress concentration, damage initiates at the hole edge with two different crack fronts, as can be seen in Fig. 5a. The cracks then propagate at angles of about 45° to the principal fibre direction (Fig. 5b), and thus follows the matrix damage developing in the adjacent 45° plies. A crack front does not localize in a plane perpendicular to the fibres in the 0° ply as observed in experiments with this type of OHT specimen. This shows that the damage model implemented in the code is not forcing the necessary localization. In order to resolve this modelling challenge, a simple engineering procedure, based on the crack band model [30] is adopted, as explained next.

The region of potential damage in these OHT specimens under static loading is the net-tension plane. Crack initiation and propagation is expected to occur along the centre of the notched cross-section. In order to initiate this so-called localization band, a 0.40 mm wide imperfection zone is considered. The choice of this width follows from a series of numerical parametric studies carried out with respect to this key modelling parameter and accounting for the limitation of Eq. (3). This introduces a length scale that can be easily adjustable compared to other techniques and is easily implemented in any finite element code. The constitutive behaviour of the localization band is characterized by fracture energy rescaling. It was found that a 90% reduction in the critical strain energy with respect to the base value $G_{1,T,c}$ ensured the expected fracture dissipation in the localization band. The imperfection therefore triggers damage development in a central zone such that the specimen enters a softening damage mode leading to a primitive localization band. Upon further loading, the strain localization band expands. For this example, the fracture process zone elongates to 1.71% at peak stress and further to 2.26% at tensile failure.

In combination with the above energy-based regularization, the artificial viscosity regularization already mentioned ensures the mesh objectivity of the results. In addition to these refinements, the mesh was also stabilized by selecting stiffness hourglass control parameters in order to solve the problem of singularities highlighted in Fig. 6 [40].

Finally, a mesh sensitivity study with respect to the degree of laminate discretization in the region surrounding the hole was carried out to determine the influence of element size on the strength prediction. In order to capture the tensile dominated problem, it was found that elements of 0.15×0.15 mm complied with the requirements for a reliable simulation and satisfied convergence requirements. This dimension, in the transverse direction of the specimen, also ensures that the

aspect ratio of the elements in the localization band (0.40/0.15 = 2.67) is kept within reasonable limits. A total of 43556 continuum shell elements are then used in the models.

Comparison between finite element predictions resulting from the improved model and experimental data [39] and previously reported predictions [37] are shown in Fig. 7. The agreement with the experimentally observed strength is significantly improved to a difference of 12%. The overall agreement between the current results and those of [37] are very good, with the latter curve marginally softer than the new predictions. This agreement provides validation for the formulation used in the present work. The difference in maximum strength prediction is 4.5%, although no particular importance is given to this, since the two continuum damage approaches are slightly different.

Fig. 8 shows plots of the damage parameters for the longitudinally-oriented fibre failure and matrix cracking at the stress levels A and B defined in Fig. 7. Tensile failure initiates at the hole edge (Fig. 8a) and propagates throughout the cross-section along the localization band (Fig. 8b). Eventually, the tensile failure band deviates from the plane of symmetry, after which the assumption of symmetric response is no longer valid. Matrix cracking initiates on the hole boundary in the plies oriented at 90° (Fig. 8c). As fibre-tension damage propagates, matrix cracking quickly extends to the outer-edge, as shown in Fig. 8d. Note that matrix cracking development extends well beyond the narrow localization band.

Similarly obtained numerical results for the $[0/\pm45/90_7]_s$ and $[0/(\pm45)_3/90_3]_s$ layups are shown in Fig. 9. As expected, both laminates experience failure along the net-section plane within the localization band of the model. The results show a similar form of tensile stress-end displacement plot to that presented in Fig. 7. The difference in strength prediction to the experiments is now –8.3% and 15% for the $[0/\pm45/90_7]_s$ and $[0/(\pm45)_3/90_3]_s$ layups, respectively. Comparisons with previously reported numerical predictions [37] show differences of –0.9% and –3.2%. This provides confidence in the finite element modelling methodology being employed.

3.3. ±45° layup

Failure of ±45° layup composites is significantly different from the previously analysed layups since nonlinear shear behaviour becomes very important to the strength prediction. The predicted tensile stress-end displacement response is presented and compared to the experimental data [39] in Fig. 10 and is observed to not be as sudden as that seen in Figs. 7 and 9. Fig. 10 represents a typically matrix-dominated failure (in shear, predominantly). The strength prediction difference in

terms of numerical (115 MPa) and experimental (126 MPa) results is –9%, which is consistent with the values established above.

Fig. 11 shows the predicted damage propagation in this laminate for the two representative plies oriented at 45° and –45°. It can be seen that damage propagates in the fibre direction without fibre breakage. Initially, matrix damage is confined to the vicinity of the hole. As the tensile load increases, matrix damage extends to the free edge at an angle of 45°, as can be seen in Figs. 11a-b, resulting in total failure as shown in Figs. 11c-d.

4. Application to pultruded composite material

4.1. Introduction

In this section, a similar modelling approach as demonstrated previously for advanced composites is adopted in the context of pultruded composite plates [41]. Pultrusion is the most extensively used processing method for composite shapes and systems in construction, as it is a cost-effective manufacturing method for high production. This process feeds fibre reinforcement and a polymer resin matrix continuously through a heated die to form the required shape at rates of up to about one meter per minute. The fibre architecture is often symmetric for a balanced laminate, and involves a combination of alternating layers of unidirectional rovings (provided as continuous parallel fibre bundles) and continuous filament mats (or occasionally, a woven fabric). The rovings run along the pultrusion length and serve to impart the required higher stiffness and strengths in that direction. The principal function of the continuous filament mats is to provide continuity to the thin-walled shape through stiffness and strength in the transverse direction. The most commonly used fibres are E-glass because they have good mechanical properties and are economical. The matrix is often polyester or vinylester resin and often contains additives [42].

Ideally, when *all-composite* structural systems are manufactured, the components are modular to provide rapid and simple assembly. Mechanical fastening is the typical connection method, because: it is simple and flexible, is familiar to practitioners, and allows frames to be demountable for reuse and recycling. Thus pultruded components require holes (notches) to accept the fasteners. It has been shown in Section 3 that the introduction of structural discontinuities create stress concentrations that give rise to initiation and growth of material damage when stress redistribution by material plasticity is limited or non-existent. This clearly reduces the efficiency of notched cross-sections and increases the complexity of behaviour, compared to that of the structural members without connections (notches).

Previous research pertaining to the behaviour of notched composites and the assessment of their structural integrity has mainly focused on investigations with advanced composite laminates for aerospace applications. Understanding cannot necessarily be extrapolated to pultruded composites since typically very thin (usually less than 2 mm) carbon fibre and high-quality glass composites dominate the aerospace industry, whereas lower-quality (and larger roving) E-glass fibres are conventionally used in pultruded members which comprise plate thicknesses up to 25 mm [43] and often utilise matrix filler to reduce cost.

In this paper, pultruded rectangular plates subject to tension with open holes are considered. The OHT strength is one limit state for the design of pultruded composite structures. Although mechanical fasteners are not present in the finite element analyses, the strength results for different OHT configurations can inform designers on, for example, the minimum hole centre-to-centre spacing (gauge distance), as a function of bolt diameter, which is needed for a structural design standard [44].

Experimental results [45] from open-hole tests of pultruded glass fibre plates having thickness of 6.4 mm were selected for modelling. Figs. 12a-c show three configurations for a rectangular specimen having a width of 100 mm and free gauge length of 200 mm. One, two or three holes of diameter d_0 = 13.1 mm are located symmetrically along the central transverse plane at a gage of 25 mm (Fig. 12). All specimens failed by fibre breakage and carried a tension stress well below that of the unnotched cross-section area [45].

Finite element simulations of the OHT tests have been performed based on the modelling methodology developed in Section 3.2. The continuum shell element had five integration points through their thickness and the material is modelled using the smeared properties listed in Table 2. Using smeared properties the modelling does not distinguish between the unidirectional and mat alternating layers. Unnotched material was characterized for the properties of E_1, E_2, $f_{1,T}$ and $f_{2,T}$ reported in Table 2 [45]. The other properties with a grey-coloured background were not experimentally determined but estimated based on research expertise and values available in literature.

The finite element approach described is used to analyse the fibre breakage dominated progressive failure process. The quantitative and qualitative accuracy of the numerical predictions are assessed by comparing these with experimental test results [45], in terms of stress-strain responses and ultimate failure modes. The specimens for the three configuration illustrated in Figs 12a-c are labelled according to the system *t-n-d-*p_2, in which *t* is the nominal thickness of the plate given in 100^{ths} of an inch, i.e. 25 is for 0.25 in. or 6.4 mm, *n* is the number of holes, *d* is the nominal bolt diameter, given in 100^{ths} of an inch, to be used in 1/64 in. or 0.4 mm clearance holes, and p_2 is

the bolt gauge, again given in 100^{ths} of an inch [45]. Each configuration had a batch of five or more specimens (labelled A, B and so forth).

4.2. Principal results with pultruded material

Experimental behaviour from [45] for the three configurations is presented in comparison with finite element predictions in Table 3 and Fig. 13. In Table 3, the notch strength reduction factor k is given as the ratio of the maximum predicted stress to the unnotched strength. Fig. 13 shows the stress-strain relationships of the three plate specimens. (The stress results correspond to the applied load averaged over the gross cross-section and the strain is the relative change in length of the plate due to the applied end displacements, i.e. $2\delta/L$.) Results from one or two of the specimens from a batch of five are shown. The figures give k and $\Delta\sigma$ for the difference in stress between notched failure and the unnotched material strength of 425 N/mm^2.

In Figs. 13a-c the general response of the tensile stress-strain curve agrees well with the experimental data over the entire loading range for the selected case studies illustrated in Figs. 12a-c. This behaviour is generally characterized by a stiff elastic phase up to failure. The numerical curves exhibit slight nonlinearity from the very beginning, and show a clear reduction in stiffness at about ⅓ of the maximum tensile load. The graphs reveal a significant effect of the interaction when there is more than one hole. The tensile strength is highest for the single hole specimen (Fig. 13a and Table 3) compared to the multiple holes plates (Figs. 13b-c and Table 3). For the latter cases, the tensile strengths are close and about 30% lower, which suggests that the drop in strength is particularly severe when there are two or more holes at the same centre-to-centre spacing (p_2) and yet it may be independent of the number of holes. From Table 3, the notch strength reduction factors (k) of 0.72, 0.52 and 0.48 further support the observation on trend.

The fibre-tension damage contour plots for the various plate configurations are shown in Figs. 14 through 20. Note that the computational models for those plates with multiple holes did not use symmetry boundary conditions. The DAMAGEFT distributions at collapse are seen to be larger at the centre of the notched cross-section (also see Cunningham *et al*. [45] for visual inspection of the fracture surfaces in specimens), as can be seen in Figs. 14, 16 and 18. For multiple hole specimens, complete fibre-tension damage first occurs between holes, at about 70% of the maximum load (see Figs. 15 and 17) and then propagates to the plate edges (see Figs. 16 and 18). These results again demonstrate that the effect of the holes interaction is quite relevant when p_2 is about $2d_0$ (d_0 is 13.1 mm). Note that p_2 of $2d_0$ is half the minimum gauge distance of $4d$ (d is 12.7 mm) specified as

mandatory in an American pre-standard [46], which is in the Standards Committee stage of preparation.

4.3. Parametric study of the plate geometry: effect of the gauge distance

The results described in Section 4.1 demonstrate the general performance of the Abaqus model in predicting the response of a pultruded plate of 6.4 mm thickness with one of more holes of 13.1 mm diameter across the section. Using this capability to predict tensile stress-strain responses reliably, the numerical study is extended to investigate different values for transverse hole spacing not covered in the experimental programme [45].

Specimen 25-2-50-100 is the baseline configuration (see Fig. 12b) selected for a parametric study. In order to quantify the effect of different edge distances, four models are built from the original, by varying the ratio p_2/d_0 (see Table 4). This ratio is varied from 1.9, corresponding to the baseline configuration tested, to a maximum of 3.5 (Test 4). Three intermediate values between these two limits of p_2/d_0 = 2.4 (Test 1), = 2.75 (Test 2) and = 3.0 (Test 3) are considered. Ratio 2.4 corresponds to the minimum design value for the design of metallic structures [47]. The other p_2/d_0 ratios are chosen for a parametric study to find out when the spacing is large enough for there to be no load path interaction between a pair of equal diameter holes.

The edge distance e_2 for the bolting is kept constant at $2.86d_0$; thus the width of the plate is increased for each virtual test (Table 4). The finite element analyses are conducted using the mechanical properties listed in Table 2. Models were assigned with symmetric boundary conditions in the thickness direction and at the centre plane in order to reduce the model size. For the OHT parameters in the models for Tests 1 to 4 the mode of failure will be due to initiation and progressive growth of fibre-tension damage.

It can be seen from Table 4 that when bolt spacing is 1.9 and $2.4d_0$, k is about 0.52 and that for the three higher spacing k is about 0.62. To explain the sudden 20% increase in strength Figs. 19 and 20 are for fibre-tension damage plots at ultimate failure, with part a for complete damage between through-thickness holes (tensile strength) and part b for propagation of damage between holes. Figs. 19a-b are for Test 1, having p_2/d_0 = 2.4, and Figs. 20a-b are for Test 3 with p_2/d_0 = 3.0. For these four damage plots it is clear that the efficiency gain is from a change in failure mechanism with increasing p_2/d_0 ratio. For $p_2/d_0 < 2.75$ damage initiates and propagates across the material *between* the pair of holes (see Fig. 19). In Fig. 20 with p_2/d_0 = 3.0, the initiation location is seen to change to the outside of the hole and propagates towards the free edge. For the higher hole spacing it is found that there is virtually no damage occurring between the holes.

This preliminary finding it is noteworthy, indicating that, providing p_2/d_0 is greater than 3.0 is sufficient to mitigate load path interaction between holes used for mechanical fastenings. This computationally-derived limit on spacing for a pultruded flat sheet material does not conflict with the existing mandatory requirement for bolted connections that the minimum p_2/d_0 is 4.0 [48].

5. Summary of modelling guidance for laminated composite materials

In this study, a progressive damage approach for composite materials has been adopted using only the predictive capabilities of the general purpose software Abaqus. This results from a combination of the prediction of damage initiation by means of the Hashin failure theory and a material damage model to simulate loss in the load-carrying capability of the part and advances the progression of damage based on mode-specific strain energy release rates. The following guidelines are provided to address common problems faced by analysts:

1. Boundary conditions consistent with the geometric symmetry of the plates can and should be employed but not on the longitudinal direction as the conditions restraining movement may change the stress field.
2. Loads should be applied by imposing incremental displacements, as opposed to the classical load control method.
3. Global stabilization and artificial viscosity prevent numerical instabilities. The values proposed in this study are 2×10^{-4} and 1×10^{-5}, for the two coefficients (respectively).
4. By using implicit methods, the mesh density that ensured convergence to the “actual” results implies a minimum of 120 elements around the hole, corresponding to the element sizes adopted in our models (see Sections 3 and 4).
5. The crack band width should be at least 1.25 times wider than the surrounding elements in the mesh.

6. Conclusions

Computational structural simulation has been used to analyse fibre-tension dominated failures in composite materials that was observed in physical and numerical tests of OHT tests of carbon/epoxy laminates for aerospace composites [37,39], and pultruded glass fibre plates intended

for civil infrastructure [45]. In this study, a progressive damage approach for composite materials has been adopted using only the predictive capabilities of the general purpose software Abaqus. This results from a combination of the prediction of damage initiation by means of the Hashin failure theory and a material damage model to simulate loss in the load-carrying capability of the part and advances the progression of damage based on mode-specific strain energy release rates.

It is shown that the proposed finite element approach is able to represent all the main features of the structural behaviour of carbon/epoxy and pultruded glass fibre plates with open holes. In particular, it offers a reliable alternative to physical testing and to complex modelling that often relies on proprietary user-subroutines to define the material mechanical behaviour. Additionally, the model can be used to fill gaps in the available data pertaining to the ultimate behaviour of these plate types and eventually assist in the implementation and application of a comprehensive set of parametric studies of plate geometry that will provide information for derivation of appropriate design requirements, say for bolt spacing in connections between pultruded plates.

This paper expands previous research by using state-of-the-art solution techniques and composite modelling provided by Abaqus. It also provides guidelines and addresses common problems faced by analysts.

Acknowledgments

This paper was produced in the framework of the project *Structural joints for building frames of pultruded fibre reinforced polymers*. This research was supported by a Marie Curie Intra European Fellowship within the 7th European Community Framework Programme under contract grant PIEF-GA-2012-327142.

References

[1] Turvey GJ, Wang P. Open-hole tension strength of pultruded GRP plate. ICE Struct Build 2003; 156(1):93-101.

[2] Abaqus Manual, Version 6.13 Dassault systems, http://www.simulia.com, 2013.

[3] Lemaitre J. Local approach of fracture. Eng Fract Mech 1986;25:523-537.

[4] Schwarze M, Reese S. A reduced integration solid-shell finite element based on the EAS and the ANS concept – Geometrically linear problems. Int J Numer Meth Eng 2009;806:1322-1355.

[5] Parisch H. A continuum-based shell theory for non-linear applications. Int J Numer Meth Eng 1995;38:1855-1833.

[6] Hauptmann R, Schweizerhof K. A systematic development of “solid-shell” element formulations for linear and non-linear analyses employing only displacement degrees of freedom. Int J Numer Meth Eng 1998;42:49-69.

[7] Hauptmann R, Schweizerhof K, Doll S, Extension of the “solid-shell” concept for application to large elastic and large elastoplastic deformations. Int J Numer Meth Eng 2000;49:1121-1141.

[8] Remmers JC, Wells GN, de Borst R. A solid-like shell element allowing for arbitrary delaminations. Int J Numer Meth Eng 2003;58:1701-1736.

[9] Hashin Z. Analysis of composite materials. J Appl Mech 1983;50:481-505.

[10] Jones RM. Mechanics of composite materials (second ed.). Taylor and Francis, USA, 1999.

[11] Kelly A, Zweben C, editors. Comprehensive composite materials, Vol. 2. Elsevier Science, 2000.

[12] Pinho A, Robinson P, Iannucci I. Fracture toughness of the tensile and compressive fibre failure modes in laminated composites. Compos Sci Technol 2006;66: 2069–2079

[13] Knops M. Analysis of failure in fiber polymer laminates – the theory of Alfred Puck. Springer, Germany, 2008.

[14] Puck A, Schürmann H. Failure analysis of FRP laminates by means of physically based phenomenological models. Compos Sci Technol 2002;62:1633-1662.

[15] Tsai SW, Wu EM. A general theory of strength for anisotropic materials. J Compos Mater 1971;5(1):58-80.

[16] Hashin Z, Rottem A. A fatigue failure criterion for fiber reinforced materials. Report AFOSR-TR-73-0686, Department of Materials Engineering, Technion – Israel Institute of Technology, 1973.

[17] Hashin Z, Failure criteria for unidirectional fiber composites. J Appl Mech 1980;47:329-334.

[18] Murray YD. Theory and verification of the fiber composite damage model implemented in DYNA3D. Report DNA-TR-89-132, 1989.

[19] Barbero EJ. Introduction to composite materials design (second ed.). CRC Press, Philadelphia, USA, 2010.

[20] Ladeveze P, Le Dantec E. Damage modelling of the elementary lamina for laminated composites. Compos Sci Technol 1992;43:257-267.

[21] Matzenmiller A, Lubliner J, Taylor RL. A constitutive model for anisotropic damage in fiber-composites. Mech Mater 1995;20:125-152.

[22] Lemaitre J. A course on damage mechanics (second ed.). Springer-Verlag, Heidelberg, Germany, 1996.

[23] Lapczyk I, Hurtado JA. Progressive damage modeling in fiber-reinforced materials. Compos Part A – Appl S 2007;38:2333-2341.

[24] Maimí P, Camanho PP, Mayugo JA, Dávila CG. A continuum damage model for composite laminates, Part I: constitutive model. Mech Mater 2007;39:897-908.

[25] Flatscher Th, Pettermann HE. A constitutive model for fiber-reinforced polymer laminae accounting for plasticity and brittle damage including softening – Implementation for implicit FEM. Compos Struct 2011;93:2241-2249.

[26] Lemaitre J, Dufailly J. Damage measurements. Eng Fract Mech 1987;28:643-661.

[27] Krajcinovic D. Damage mechanics. Mech Mater 1989;8:117-197.

[28] Ju JW. Isotropic and anisotropic damage variables in continuum damage mechanics. J Eng Mech-ASCE 1990;116(12):2764-2770.

[29] Catalanotti G, Camanho PP, Xavier J, Dávila CG, Marques AT. Measurement of resistance curves in the longitudinal failure of composites using digital image correlation. Compos Sci Technol 2010;70:1986-1993.

[30] Bažant ZP, Oh BH. Crack band theory for fracture of concrete. Mater Struct 1983;16:155-177.

[31] Bažant ZP, Planas J. Fracture and size effect in concrete and other quasi-brittle materials. CRC Press, Boca Raton, USA, 1998.

[32] Bažant ZP, Jirásek M. Nonlocal integral formulations of plasticity and damage: survey of progress. J Eng Mech-ASCE 2002;128(11):1119-1149.

[33] Belytschko T, Bažant ZP, Hyun YW, Chang TP. Strain-softening materials and finite-element solutions. Comput Struct 1986;23(2):163-180.

[34] Pijaudier-Cabot G, Bažant ZP. Nonlocal damage theory. J Eng Mech-ASCE 1987;113(10):1512-1533.

[35] Jirásek M, Patzák B. Models for quasi-brittle failure: theoretical and computational aspects In: Proceedings of the 2nd European Conference on computational mechanics; solids, structures and coupled problems in engineering, 2001. P. 70-71 (full paper on CD Rom).

[36] Needleman A. Material rate dependence and mesh sensitivity in localization problems. Comput Method Appl M 1988;67:69-85.

[37] Maimí P, Camanho PP, Mayugo JA, Dávila CG. A continuum damage model for composite laminates, Part II: computational implementation and validation. Mech Mater 2007;39:909-919.

[38] Crisfield M. Non-linear finite element analysis of solids and structures, Volume 1: Essentials. John Wiley & Sons Ltd., Chichester, UK, 1997.

[39] Chang FK, Chang KY. A progressive damage model for laminated composites containing stress concentrations. J Compos Mater 1987;21:834-855.

[40] Belytschko T, Ong JSJ, Liu WK, Kennedy JM. Hourglass control in linear and nonlinear problems. Comput Method Appl M 1984;43:251-276.

[41] Starr TF, editor. Pultrusion for engineers. Woodhead Publishing Ltd., Cambridge, 2000.

[42] Bank LC. Composites for construction: Structural design with FRP materials. John Wiley & Sons, New Jersey, 2006.

[43] Wang P. Structural integrity of bolted joints for pultruded GRP profiles. PhD thesis, Lancaster Univ., 2004.

[44] Mottram JT. Design guidance for bolted connections in structures of pultruded shapes: Gaps in knowledge. In: Proceedings of the17th International Conference on Composite Materials (ICCM17), 27-31 July 2009, Paper A1:6. p. 12.

[45] Cunningham D, Harries KA, Bell AJ. Open-hole tension capacity of pultruded GFRP having staggered hole arrangement. Comp Struct (submitted for publication, 2014).

[46] Anonymous. New Pre-Standard for Pultruded FRP Composites Funded through ACMA Means Increased Applications, American Composites Manufacturers Association (ACMA) press release (2014). http://www.acmanet.org/press-releases/13-communications/240-new-pre-standard-for-pultruded-frp-composites-funded-thru-acma-means-increased-applications (December, 10, 2014)

[47] CEN – European Committee for Standardization. EN1993-1-8 Design of steel structures, Part 1-8: Design of joints. Brussels, 2005.

[48] American Composites Manufactures Association. (2012). Pre-standard for load & resistance factor design (LRFD) of pultruded fiber reinforced polymer (FRP) structures. http://www.acmanet.org/cgi-committees/pultrusion-industry-council (Dec. 18, 2014)

Figure captions list

Table captions list

Fig. 1

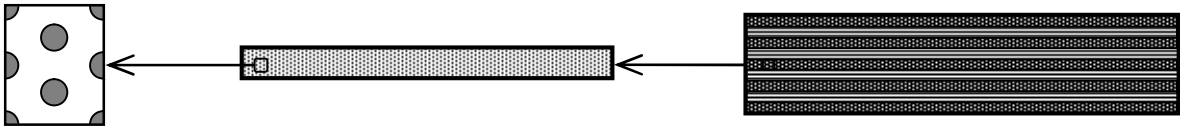

Constituents
(matrix and fibres)
Microscale

Lamina
Mesoscale

Laminate
Macroscale

Fig. 2

a)

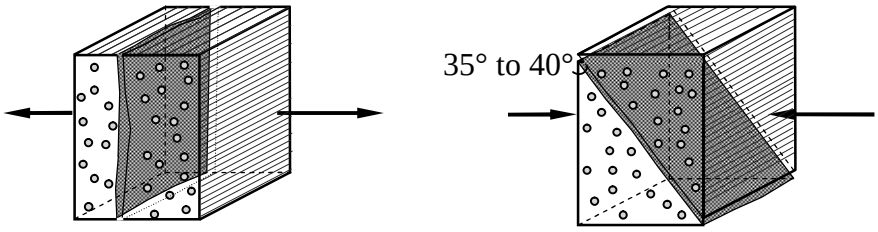

Transverse tension (mode 2,T) Transverse compression (mode 2,C)

b)

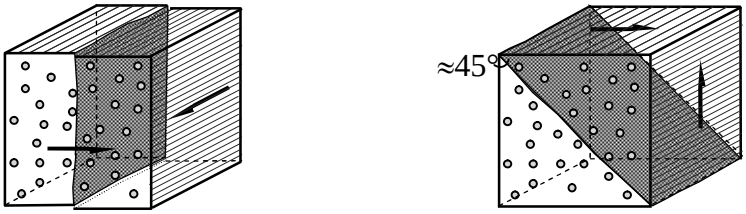

Transverse shear (mode 2,S) Longitudinal shear (mode 1,S)

c)

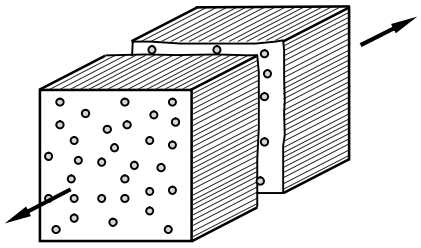

Fibre breakage

Tension (mode 1,T)

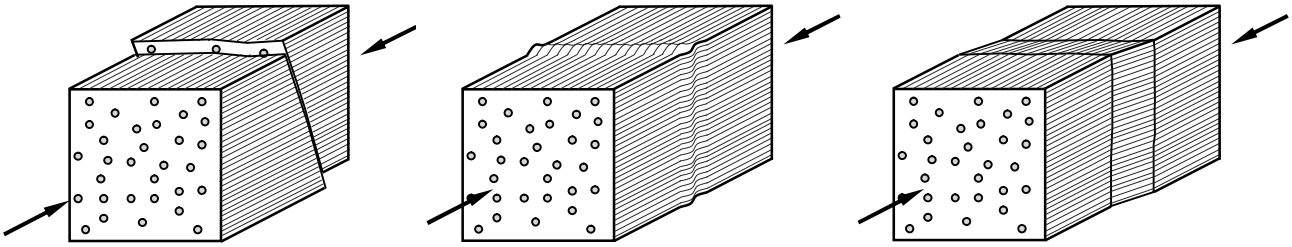

Fibre fracture in shear *Micro-buckling* *Kinking*

Compression (mode 1,C)

Fig. 3

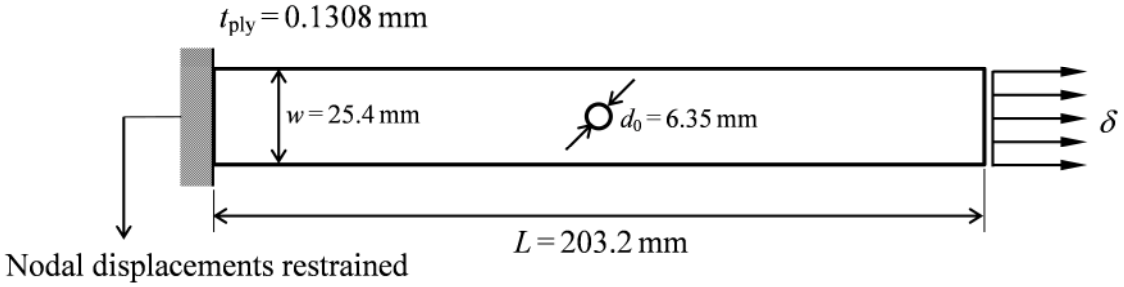
$t_{ply} = 0.1308$ mm
$w = 25.4$ mm
$d_0 = 6.35$ mm
δ
$L = 203.2$ mm
Nodal displacements restrained

Fig. 4

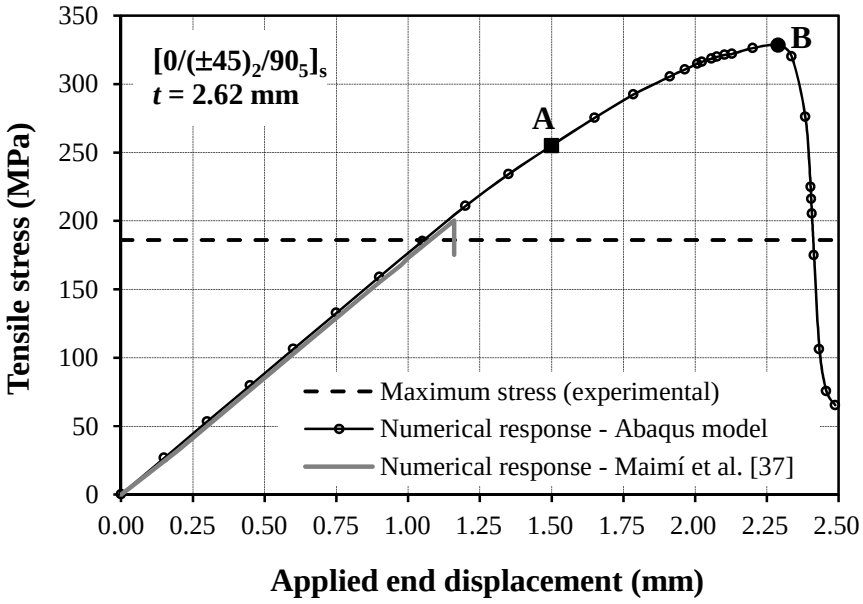
$[0/(\pm45)_2/90_5]_s$
t = 2.62 mm
A
B
Tensile stress (MPa)
Applied end displacement (mm)
Maximum stress (experimental)
Numerical response - Abaqus model
Numerical response - Maimí et al. [37]
0
50
100
150
200
250
300
350
0.00
0.25
0.50
0.75
1.00
1.25
1.50
1.75
2.00
2.25
2.50

Fig. 5

a) **b)**

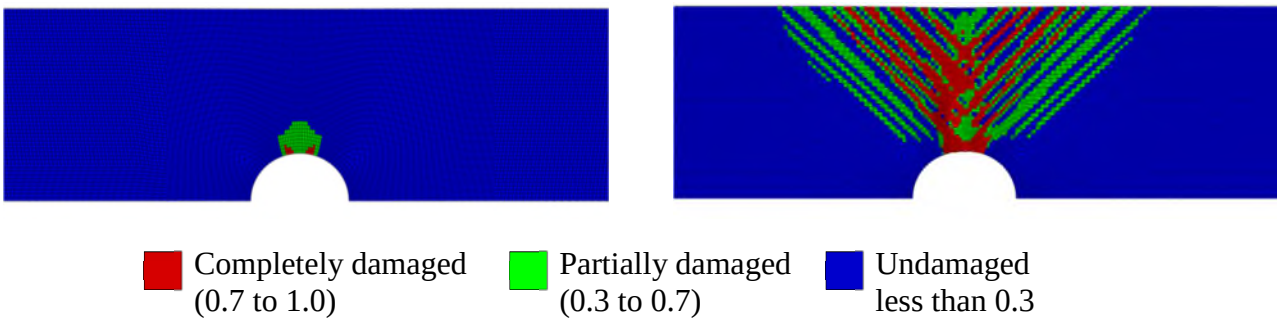
Completely damaged
(0.7 to 1.0)
Partially damaged
(0.3 to 0.7)
Undamaged
less than 0.3

Fig. 6

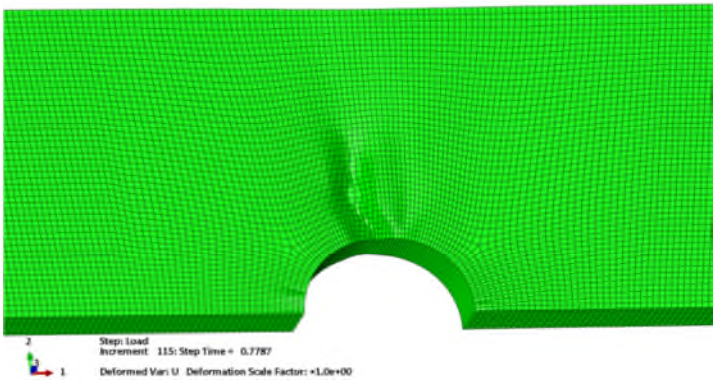
Step: Load
Increment 115: Step Time = 0.7787
Deformed Var: U Deformation Scale Factor: +1.0e+00

Fig. 7

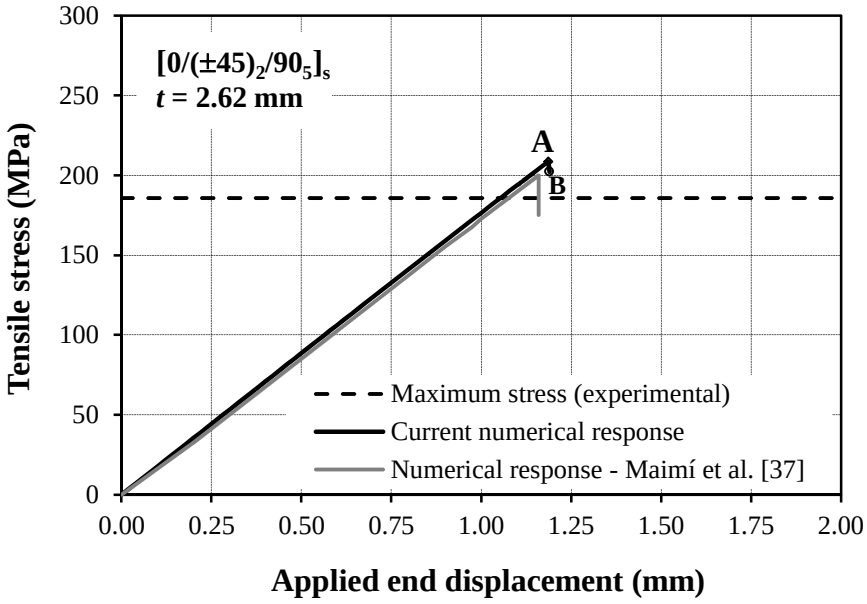
[0/(±45)2/905]s
t = 2.62 mm
A
B
Maximum stress (experimental)
Current numerical response
Numerical response - Maimí et al. [37]
Tensile stress (MPa)
Applied end displacement (mm)
300
250
200
150
100
50
0
0.00
0.25
0.50
0.75
1.00
1.25
1.50
1.75
2.00

Fig. 8

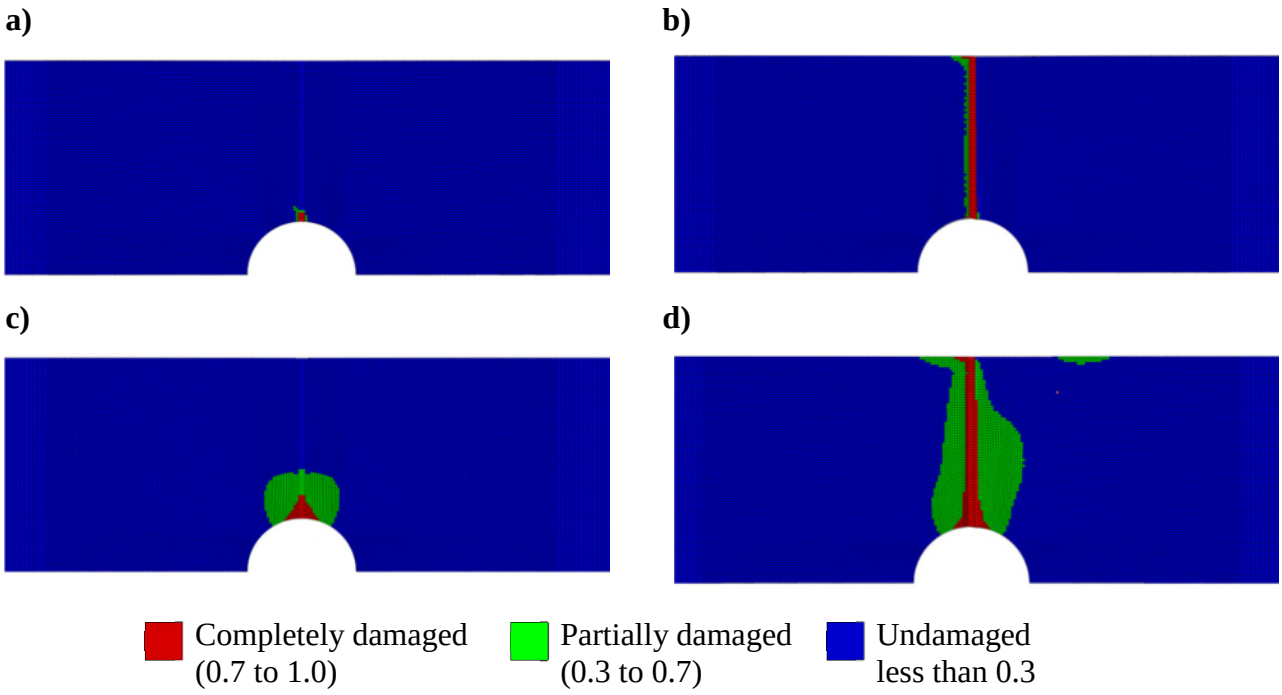
a)
b)
c)
d)
Completely damaged
(0.7 to 1.0)
Partially damaged
(0.3 to 0.7)
Undamaged
less than 0.3

Fig. 9

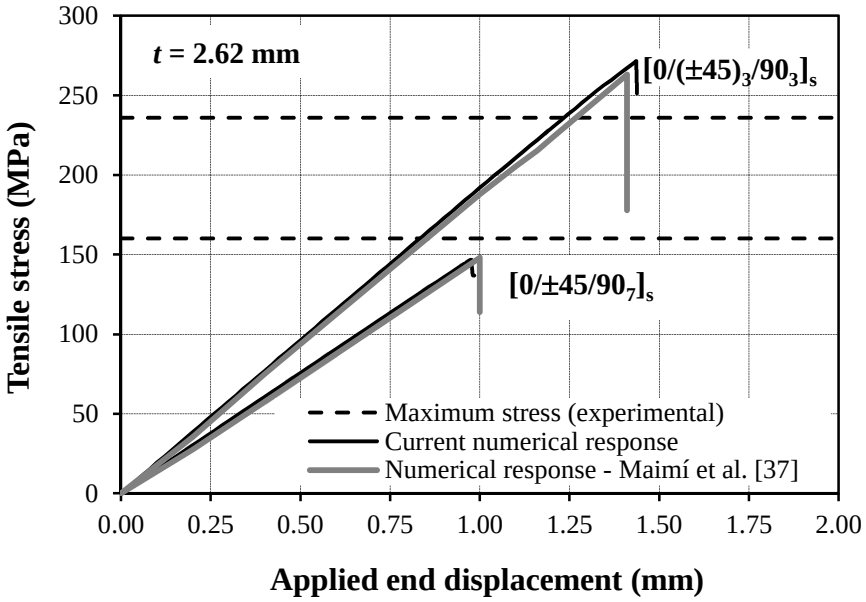
t = 2.62 mm
[0/(±45)3/903]s
[0/±45/907]s
Maximum stress (experimental)
Current numerical response
Numerical response - Maimí et al. [37]
Tensile stress (MPa)
Applied end displacement (mm)
300
250
200
150
100
50
0
0.00
0.25
0.50
0.75
1.00
1.25
1.50
1.75
2.00

Fig. 10

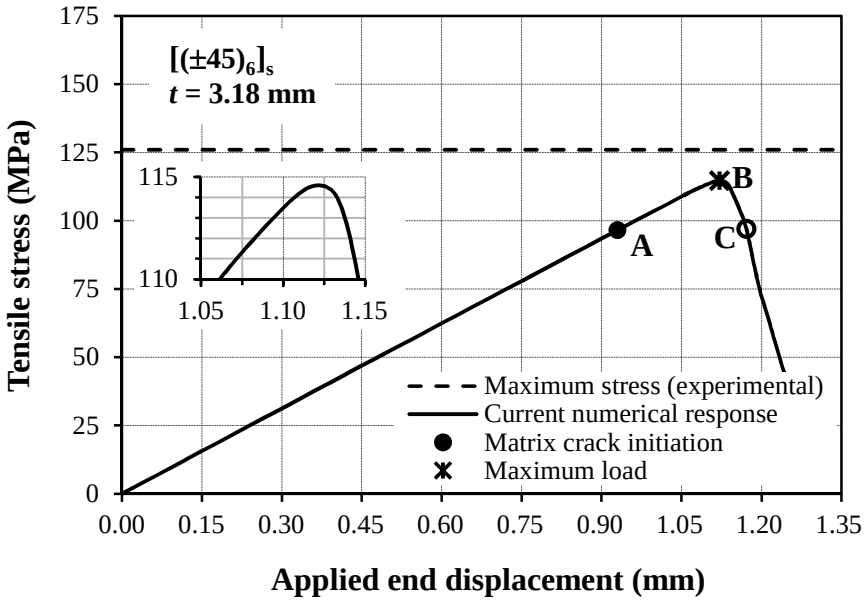
[(±45)6]s
t = 3.18 mm
Tensile stress (MPa)
Applied end displacement (mm)
Maximum stress (experimental)
Current numerical response
Matrix crack initiation
Maximum load
A
B
C
175
150
125
100
75
50
25
0
115
110
1.05
1.10
1.15
0.00
0.15
0.30
0.45
0.60
0.75
0.90
1.05
1.20
1.35

Fig. 11

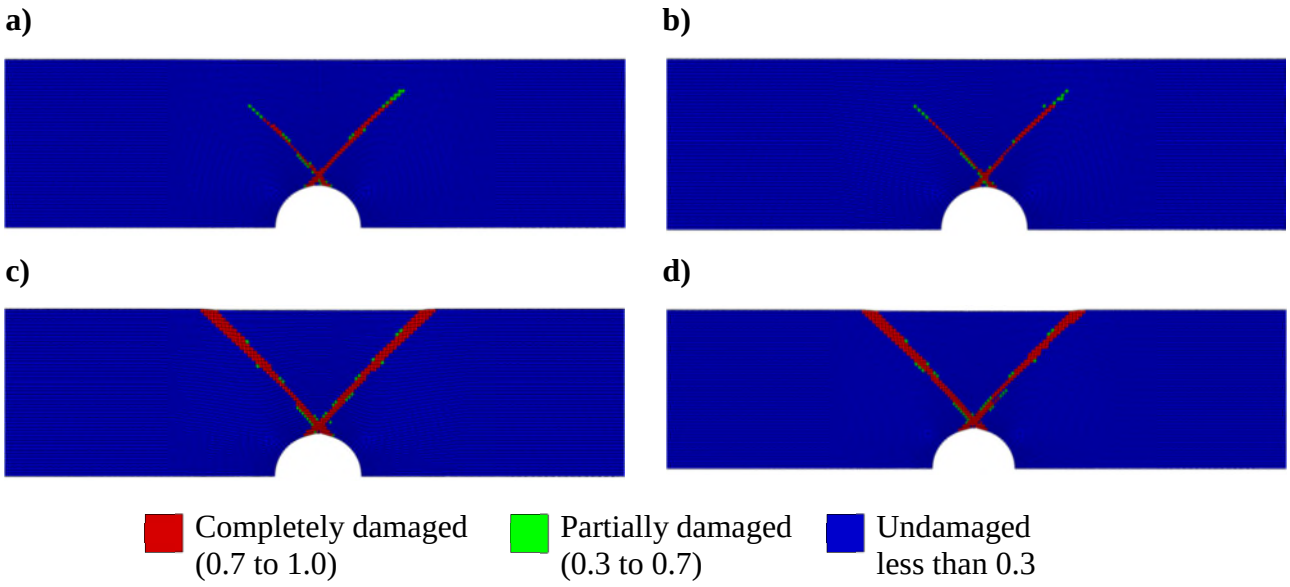
a)
b)
c)
d)
Completely damaged
(0.7 to 1.0)
Partially damaged
(0.3 to 0.7)
Undamaged
less than 0.3

Fig. 12

a)

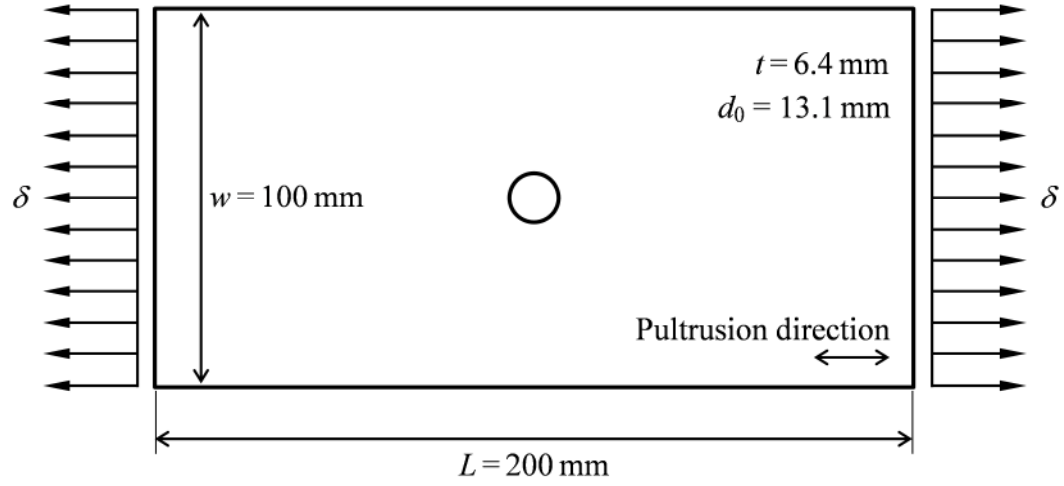
t = 6.4 mm
d0 = 13.1 mm
δ
w = 100 mm
δ
Pultrusion direction
L = 200 mm

b)

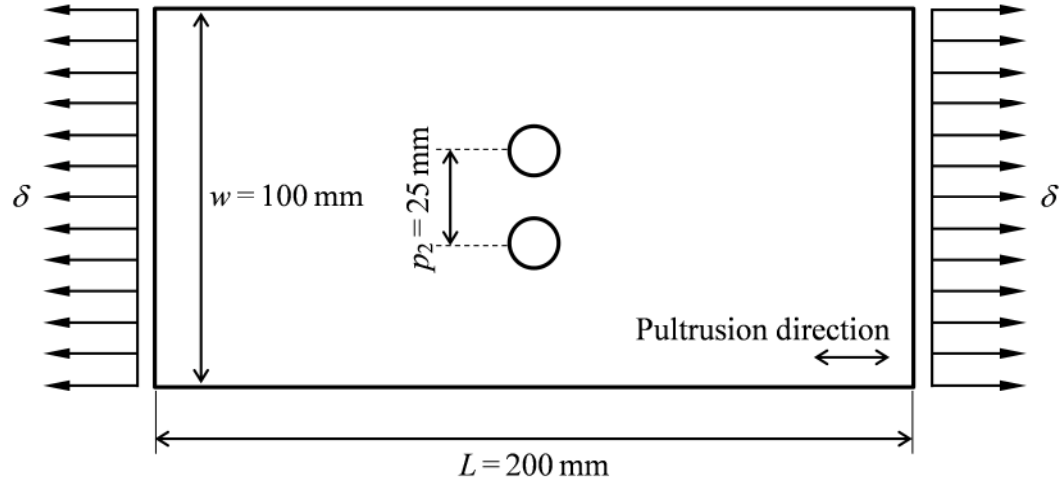
δ
w = 100 mm
p2 = 25 mm
δ
Pultrusion direction
L = 200 mm

c)

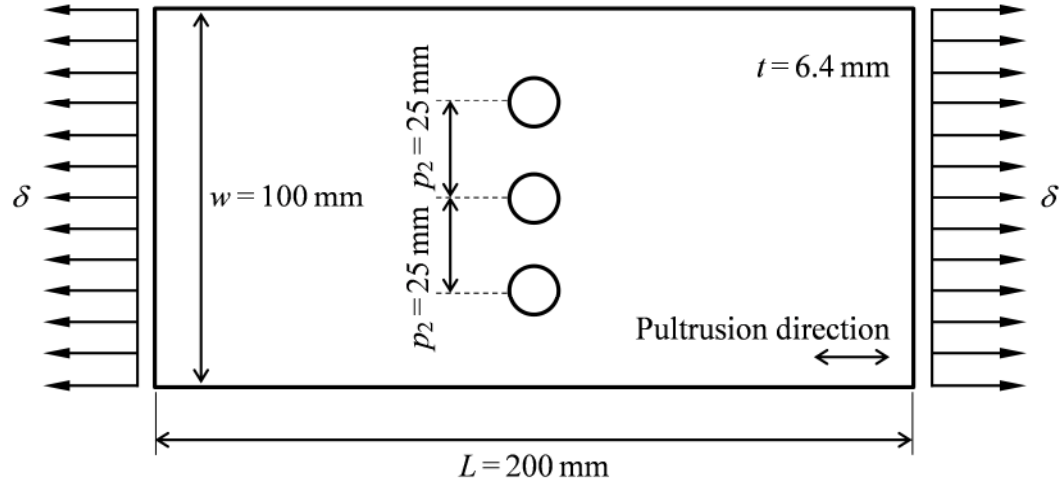
t = 6.4 mm
δ
w = 100 mm
p2 = 25 mm
p2 = 25 mm
δ
Pultrusion direction
L = 200 mm

Fig. 13

a)

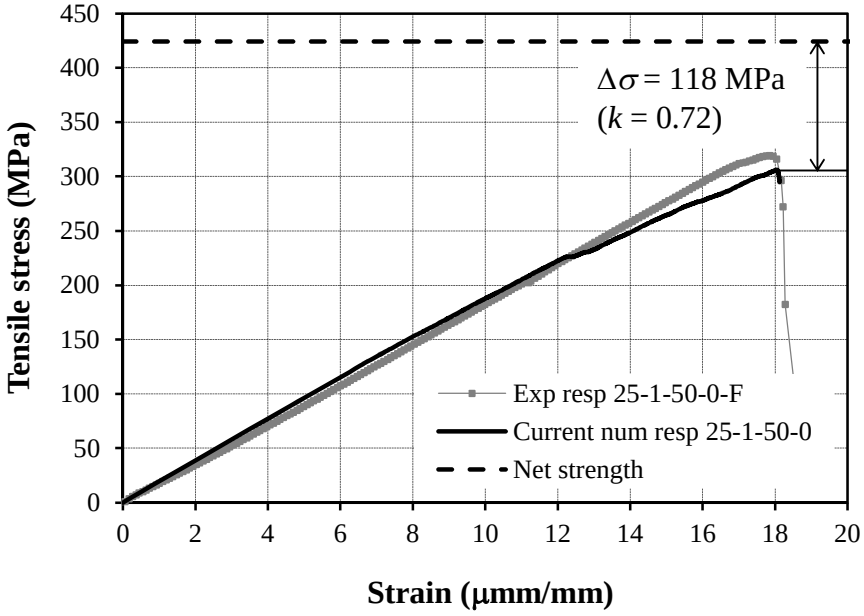
Δσ = 118 MPa
(k = 0.72)
Exp resp 25-1-50-0-F
Current num resp 25-1-50-0
Net strength
Tensile stress (MPa)
Strain (μmm/mm)
0
50
100
150
200
250
300
350
400
450
0
2
4
6
8
10
12
14
16
18
20

b)

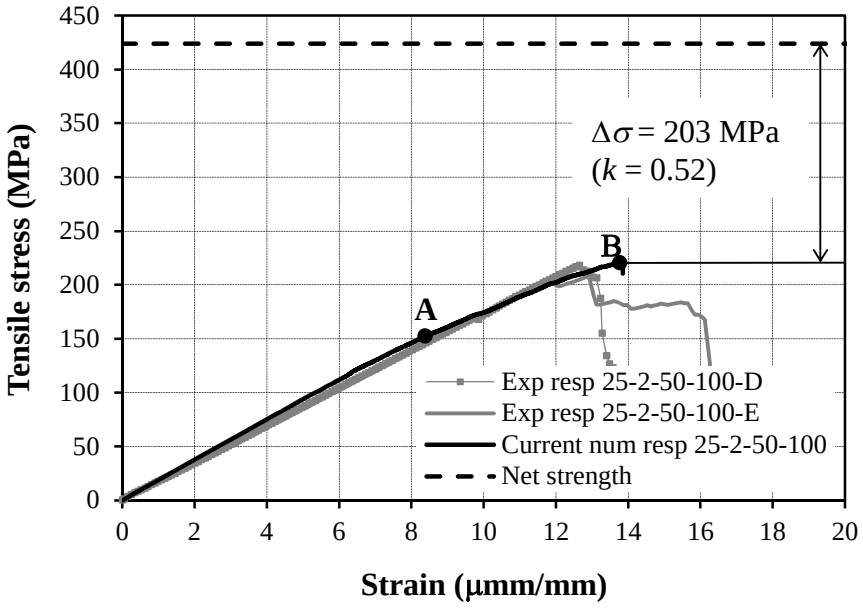
Δσ = 203 MPa
(k = 0.52)
A
B
Exp resp 25-2-50-100-D
Exp resp 25-2-50-100-E
Current num resp 25-2-50-100
Net strength
Tensile stress (MPa)
Strain (μmm/mm)
0
50
100
150
200
250
300
350
400
450
0
2
4
6
8
10
12
14
16
18
20

Fig. 13 (cont´d)

c)

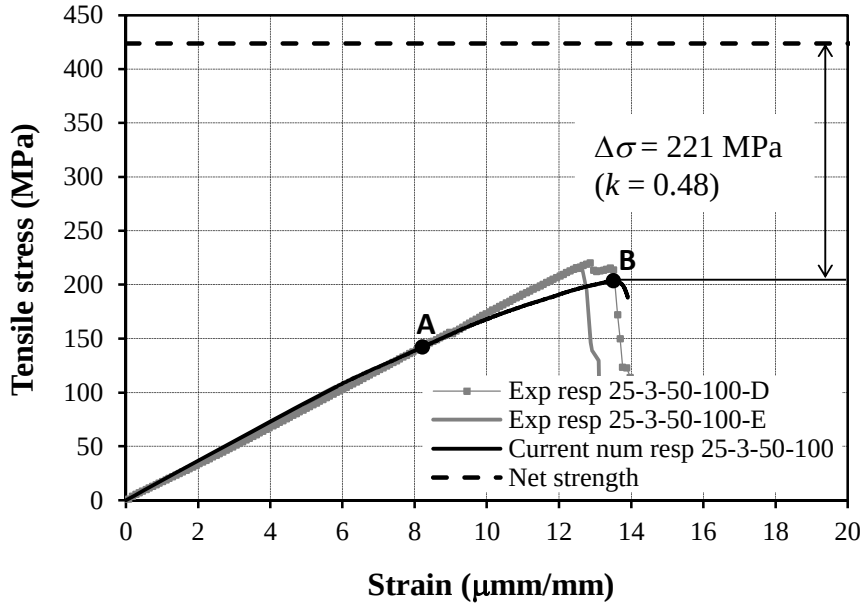

Fig. 14

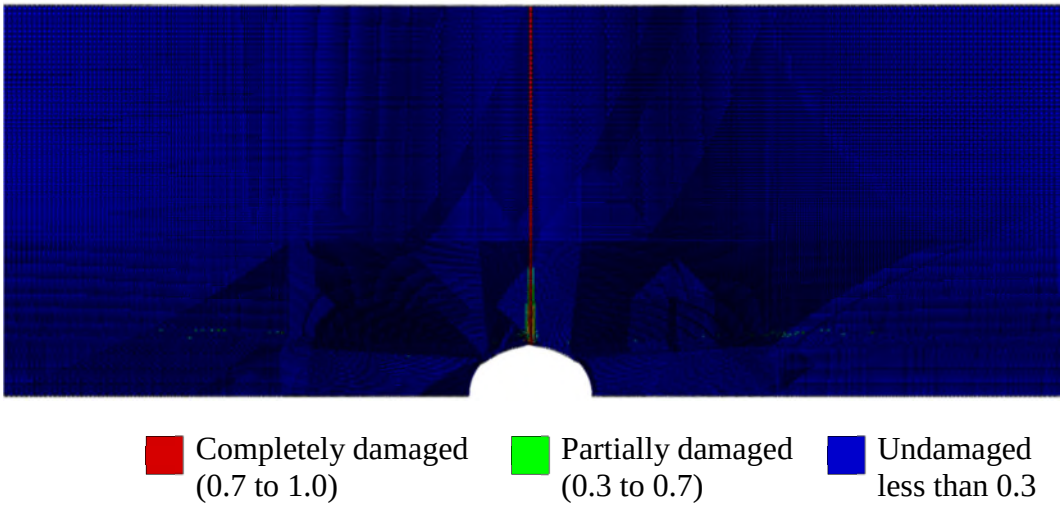
Completely damaged
(0.7 to 1.0)
Partially damaged
(0.3 to 0.7)
Undamaged
less than 0.3

Fig. 15

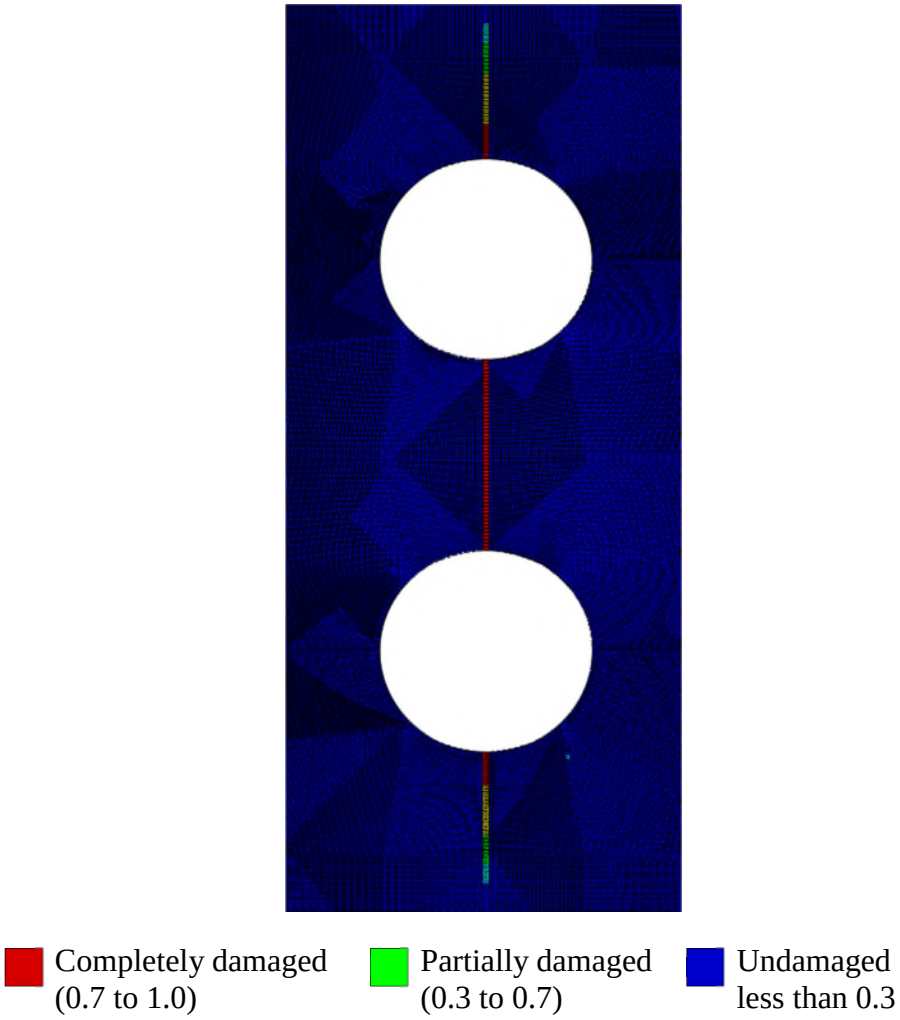
Completely damaged
(0.7 to 1.0)
Partially damaged
(0.3 to 0.7)
Undamaged
less than 0.3

Fig. 16

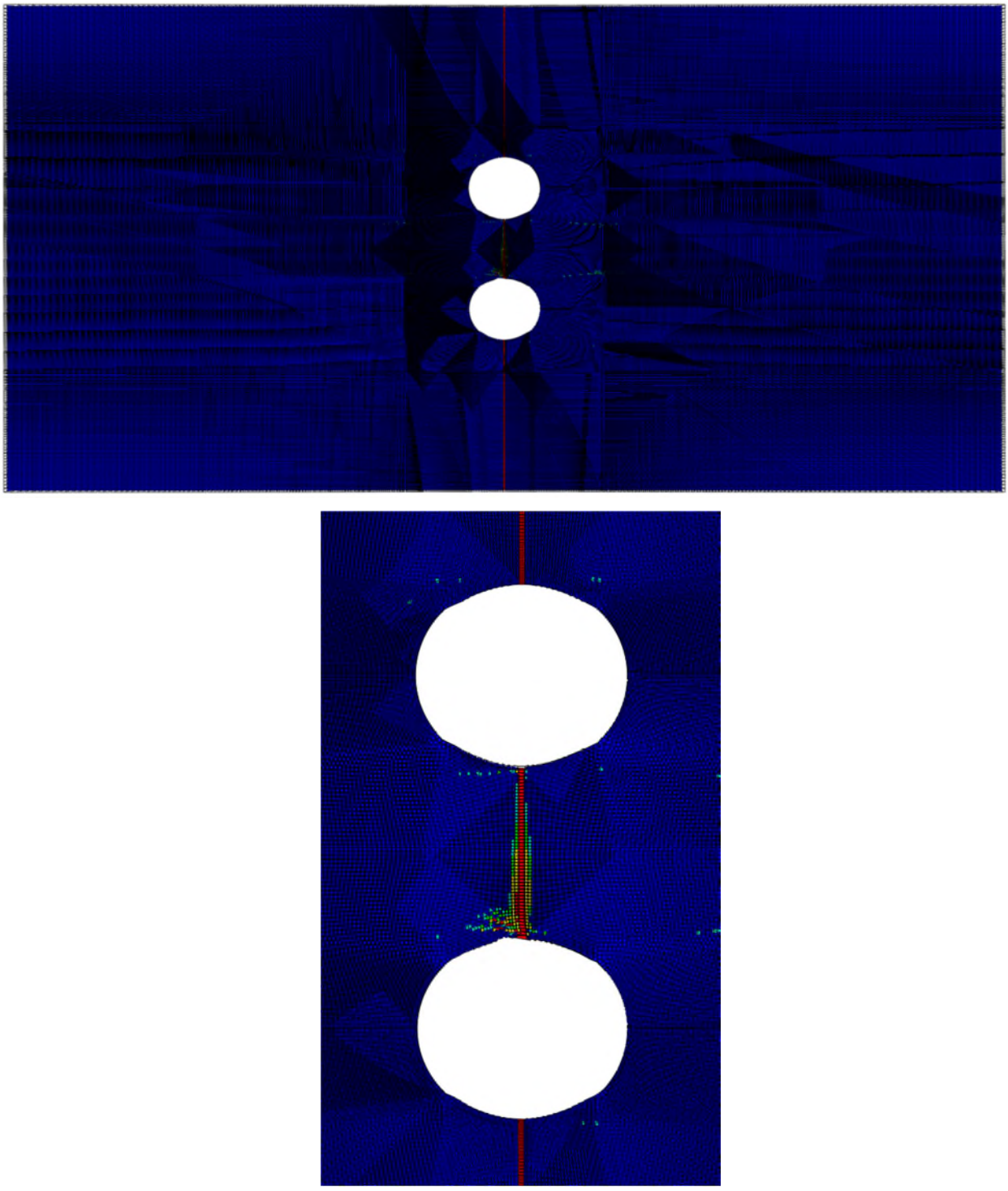
Completely damaged
(0.7 to 1.0)
Partially damaged
(0.3 to 0.7)
Undamaged
less than 0.3

Fig. 17

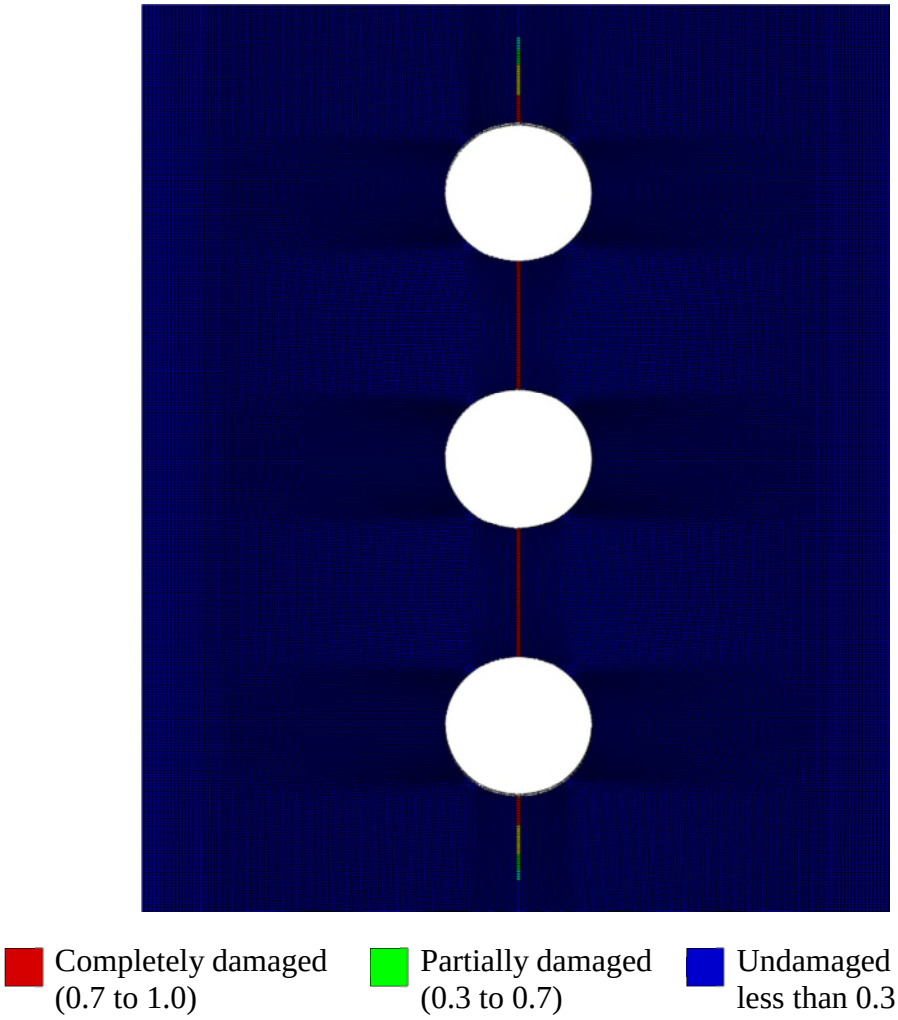
Completely damaged
(0.7 to 1.0)
Partially damaged
(0.3 to 0.7)
Undamaged
less than 0.3

Fig. 18

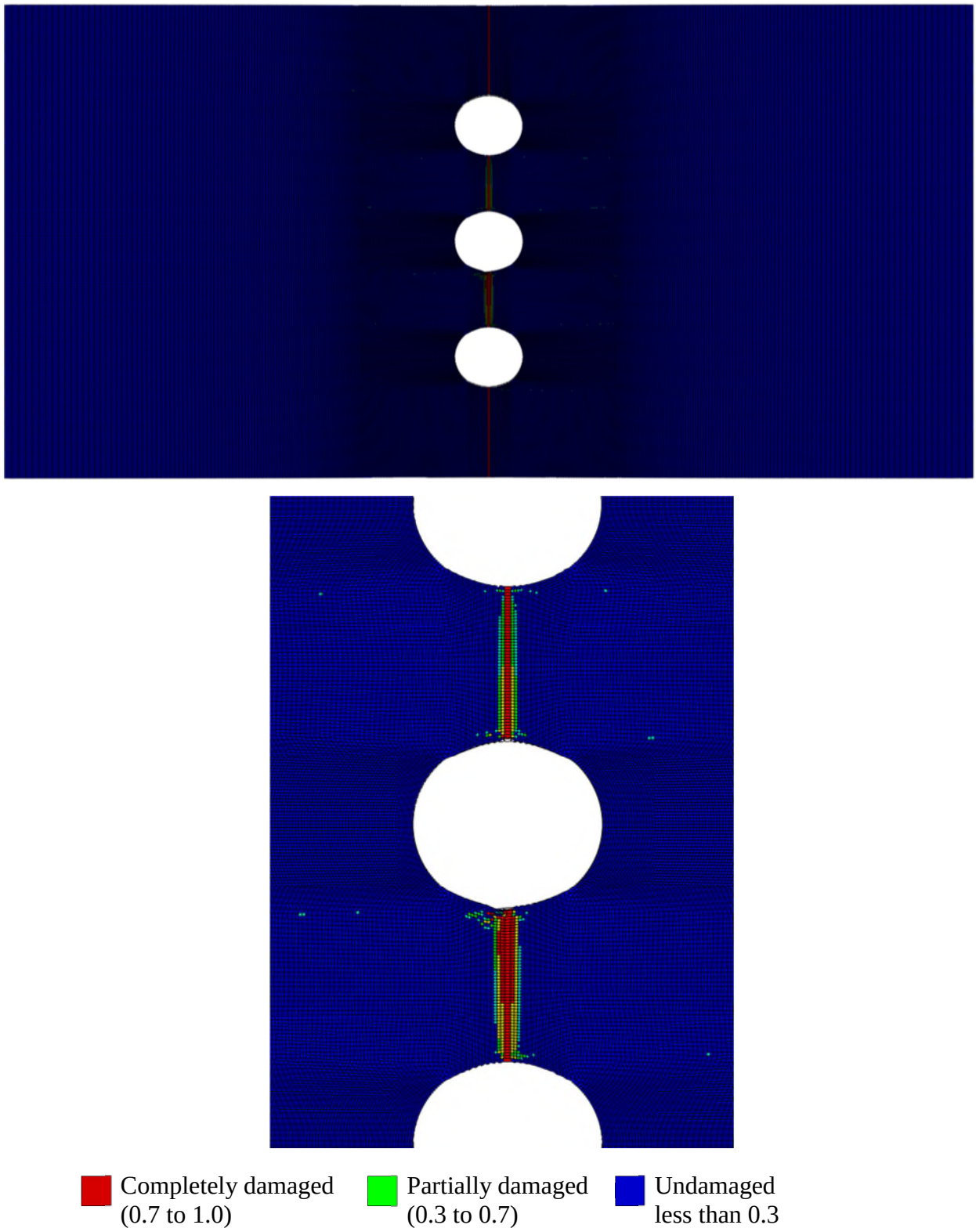
Completely damaged
(0.7 to 1.0)
Partially damaged
(0.3 to 0.7)
Undamaged
less than 0.3

Fig. 19

a)

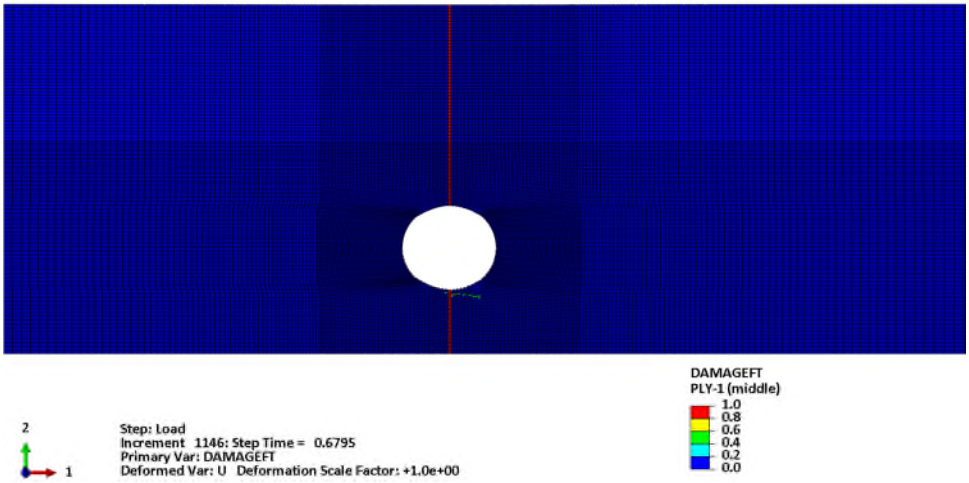

b)

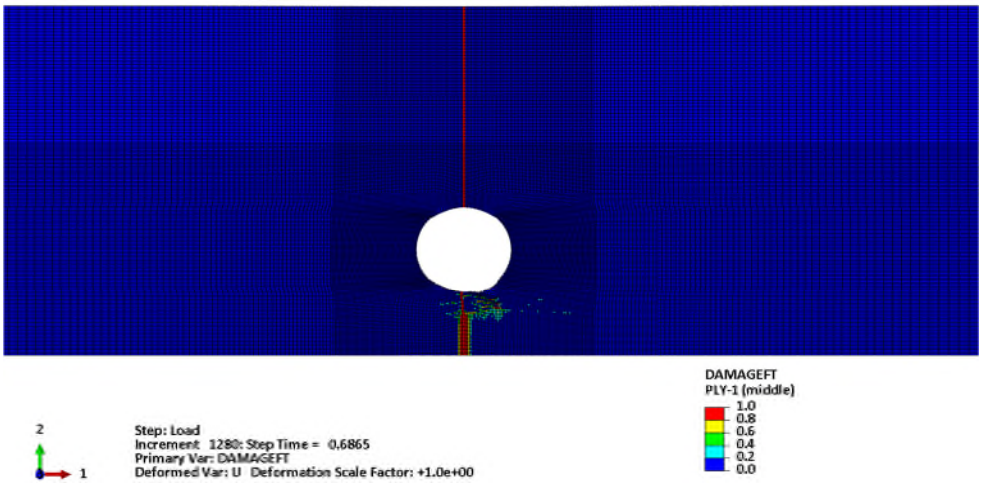

Completely damaged Partially damaged Undamaged

Fig. 20

a)

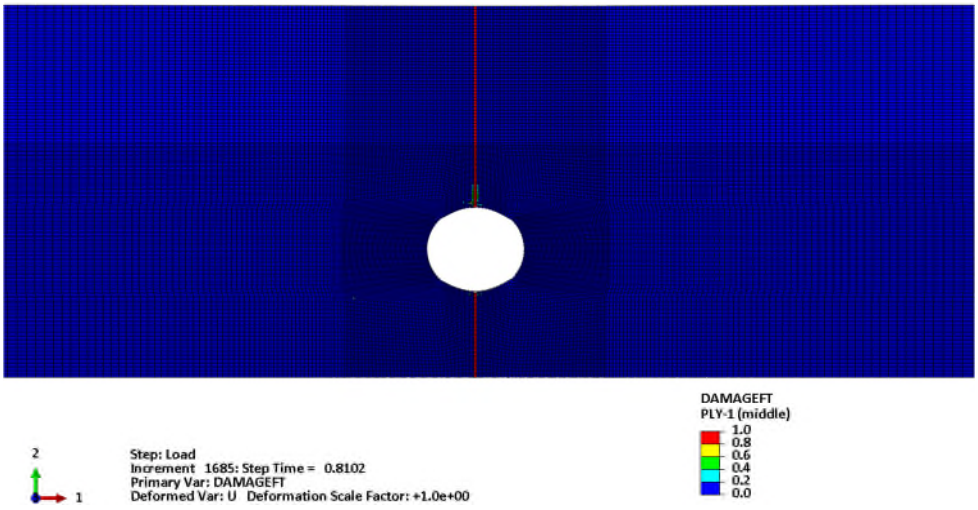

b)

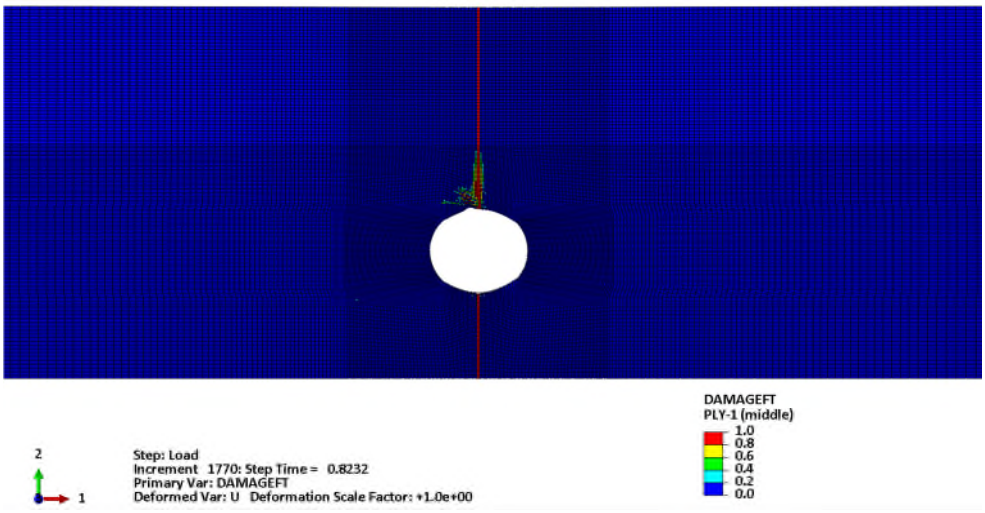

Completely damaged Partially damaged Undamaged

Table 1

Lamina elastic constants		Lamina strengths		Fracture energies	
E_1 (N/mm^2)	146800	$f_{1,T}$ (N/mm^2)	1730	$G_{1,T,c}$ (N/mm)	89.8
$E_2 = E_3$ (N/mm^2)	11380	$f_{1,C}$ (N/mm^2)	1379	$G_{1,C,c}$ (N/mm)	78.3
$G_{12} = G_{13}$ (N/mm^2)	6100	$f_{2,T}$ (N/mm^2)	67	$G_{2,T,c}$ (N/mm)	0.23
G_{23} (N/mm^2)	5500	$f_{2,C}$ (N/mm^2)	268	$G_{2,C,c}$ (N/mm)	0.76
ν_{12}	0.30	$f_{1,S} = f_{2,S}$ (N/mm^2)	59		

Table 2

Elastic lamina properties		Lamina strength properties		Fracture energy	
E_1 (N/mm^2)	19843	$f_{1,T}$ (N/mm^2)	425	$G_{1,T,c}$ (N/mm)	100
$E_2 = E_3$ (N/mm^2)	6435	$f_{1,C}$ (N/mm^2)	450	$G_{1,C,c}$ (N/mm)	100
$G_{12} = G_{13}$ (N/mm^2)	4000	$f_{2,T}$ (N/mm^2)	94.5	$G_{2,T,c}$ (N/mm)	1.2
G_{23} (N/mm^2)	3500	$f_{2,C}$ (N/mm^2)	250	$G_{2,C,c}$ (N/mm)	5
ν_{12}	0.26	$f_{1,S}$ (N/mm^2)	50		
		$f_{2,S}$ (N/mm^2)	80		

Table 3

Test	Strength (N/mm^2)				
	Finite element results			Experiments (mean)	Ratio to experiments
	Unnotched strength	Max. stress	k	Max. stress	
25-1-50-0	425	306	0.72	291	1.05
25-2-50-100	425	221	0.52	226	0.98
25-3-50-100	425	203	0.48	178	1.14

Table 4

Test	Parameter variation		Strength (N/mm^2)		
			Finite element results		
	p_2/d_0	w (mm)	Unnotched strength	Max. stress	k
25-2-50-100	1.9	100.0	425	221	0.52
Test 1	2.4	107.8	425	224	0.53
Test 2	2.75	111.0	425	270	0.64
Test 3	3.0	114.3	425	262	0.62
Test 4	3.5	120.8	425	277	0.65